



THE UNIVERSITY *of* EDINBURGH

Edinburgh Research Explorer

Age-Depth Stratigraphy of Pine Island Glacier Inferred from Airborne Radar and Ice-Core Chronology

Citation for published version:

Bodart, J, Bingham, RG, Ashmore, DW, Karlsson, NB, Hein, A & Vaughan, DG 2021, 'Age-Depth Stratigraphy of Pine Island Glacier Inferred from Airborne Radar and Ice-Core Chronology', *Journal of Geophysical Research: Earth Surface*. <https://doi.org/10.1029/2020JF005927>

Digital Object Identifier (DOI):

[10.1029/2020JF005927](https://doi.org/10.1029/2020JF005927)

Link:

[Link to publication record in Edinburgh Research Explorer](#)

Document Version:

Peer reviewed version

Published In:

Journal of Geophysical Research: Earth Surface

General rights

Copyright for the publications made accessible via the Edinburgh Research Explorer is retained by the author(s) and / or other copyright owners and it is a condition of accessing these publications that users recognise and abide by the legal requirements associated with these rights.

Take down policy

The University of Edinburgh has made every reasonable effort to ensure that Edinburgh Research Explorer content complies with UK legislation. If you believe that the public display of this file breaches copyright please contact openaccess@ed.ac.uk providing details, and we will remove access to the work immediately and investigate your claim.



Age-Depth Stratigraphy of Pine Island Glacier Inferred from Airborne Radar and Ice-Core Chronology

J. A. Bodart^{1,4*}, R. G. Bingham¹, D. W. Ashmore², N. B. Karlsson³, A.S. Hein¹, and D. G. Vaughan⁴

¹ School of GeoSciences, University of Edinburgh, Edinburgh, UK.

² School of Environmental Sciences, University of Liverpool, Liverpool, UK.

³ Geological Survey of Denmark and Greenland, Copenhagen, Denmark.

⁴ British Antarctic Survey, Cambridge, UK.

*Corresponding author: Julien Bodart (julien.bodart@ed.ac.uk)

Key Points

- Using airborne radar, we trace four isochronous internal reflecting horizons over Pine Island Glacier, West Antarctica
- Isochrone ages calculated using the WAIS Divide ice core and a 1-D model are 2.31-2.92, 4.72 ± 0.28 , 6.94 ± 0.31 , and 16.50 ± 0.79 ka
- We show that these isochrones are widespread across Pine Island Glacier and extend into neighbouring Weddell and Amundsen Sea regions

Abstract

Understanding the contribution of the West Antarctic Ice Sheet (WAIS) to past and future sea level has been a major scientific priority over the last three decades. In recent years, observed thinning and ice-flow acceleration of the marine-based Pine Island Glacier has highlighted that understanding dynamic changes is critical to predicting the long-term stability of the WAIS. However, relatively little is known about the evolution of the catchment during the Holocene. Internal Reflecting Horizons (IRHs) provide a cumulative record of accumulation, basal melt and ice dynamics that, if dated, can be used to constrain ice-flow models. Here, we use airborne radars to trace four spatially-extensive IRHs deposited in the late Quaternary across the Pine Island Glacier catchment. We use the WAIS Divide ice-core chronology to assign ages to three IRHs: 4.72 ± 0.28 , 6.94 ± 0.31 , and 16.50 ± 0.79 ka. We use a 1-D model, constrained by observational and modelled accumulation rates, to produce an independent validation of our ice-core-derived ages and provide an age estimate for our shallowest IRH (2.31-2.92 ka). We find that our upper three IRHs correspond to three large peaks in sulphate concentrations in the WAIS Divide ice-core record and hypothesise that the origin of these spatially-extensive IRHs is from past volcanic activity. The clear correspondence between our IRHs and the ones previously identified over the Weddell Sea Sector, altogether representing ~20% of the WAIS, indicates that a unique set of stratigraphic markers spanning the Holocene exists over a large part of West Antarctica.

Key Words: Pine Island Glacier, Holocene, Ice Penetrating Radar, West Antarctica, Englacial Stratigraphy, Thwaites Glacier

1 Introduction

The West Antarctic Ice Sheet (WAIS) has been losing mass at an accelerating rate since satellite records began, averaging 94 ± 27 Gt yr⁻¹ of mass loss since 1992 (Shepherd et al., 2018). Approximately 40% of this loss was through Pine Island Glacier (PIG), which alone has contributed ~3 mm of the total ~7 mm sea-level-rise contribution of the WAIS between 1979 and 2017 (Rignot et al., 2019). The increasing mass-loss trend of PIG has been primarily driven by interannual and decadal-scale atmospheric and oceanic forcing, triggering grounding-line retreat and consequent inland dynamical adjustments (Bodart and Bingham, 2019; Christianson et al., 2016; Dutrieux et al., 2014; Favier et al., 2014; Holland et al., 2019; Konrad et al., 2017; Rignot et al., 2019; Smith et al., 2017). However, placing the observed changes over the last four decades within the context of longer-term dynamic changes and sea-level rise contribution is challenging (Medley et al., 2018; Palermé et al., 2017), as the short observational satellite record captures only slight perturbations in the forcing and response which are not sufficient to predict a future in which changes are likely to be rapid and large. This lack of long-term observations currently limits our understanding of the likely future evolution of this sensitive sector of the WAIS. Reaching further back into the past will help us capture a wider set of ice-sheet configurations, and so create a more robust basis for future predictions of the Antarctic Ice Sheet evolution (Bracegirdle et al., 2019; DeConto and Pollard, 2016; Ritz et al., 2001).

Past research has focused primarily on using in situ observations and ice-sheet models to reconstruct the evolution of the WAIS since the Last Glacial Maximum (LGM, ~20 ka BP), indicating that WAIS contained significantly more ice than at present, with the potential to have raised sea level by more than 9 m at the LGM (Denton and Hughes, 2002). Several studies have reported evidence of short-lived episodes of rapid grounding-line retreat in the Amundsen Sea Embayment (ASE) between the LGM and the start of the Holocene (~11.5 ka BP) (Hillenbrand et al., 2013; Jakobsson et al., 2011; Lowe and Anderson, 2002). However, much less is known about the interior ice-sheet history of this region during the Holocene. Cosmogenic nuclide studies on isolated nunataks across the ASE suggest significant ice thinning occurred during the early- to mid-Holocene in the central ASE (Johnson et al., 2017; 2020; Lindow et al., 2014), with thinning complete by the mid-Holocene in the eastern ASE near PIG (Johnson et al., 2008; 2014). More recent evidence, based on sediment cores, ice-penetrating radar and ice-sheet modelling, showed possible retreat and re-advance of the WAIS grounding line over millennial timescales during the Holocene (Kingslake et al., 2018), although evidence of such behaviour is not available in the ASE region.

Internal Reflecting Horizons (IRHs), as observed by ice-penetrating radars, provide a powerful and complementary resource to point-based geochronological measurements. Excluding basal ice and erosional surfaces, the majority of specular, continuous IRHs are isochronous (Whillans, 1976); many can be traced for several hundreds of kilometres and provide a record of accumulation rates and patterns, convolved with key information on past ice-dynamical processes (Bingham and Siegert, 2007; Eisen et al., 2005; 2008; Siegert et al., 1998). IRHs can thus serve as a valuable resource for constraining past changes in surface mass balance and ice-flow velocities (e.g. Rotschky et al., 2004), and, where they can be dated, can be incorporated into ice-flow models, as previously shown for Greenland (Fahnestock et al., 2001a; MacGregor et al., 2016) and Antarctica (Cavitte et al., 2018; Leysinger Vieli et al., 2011; Koutnik et al., 2016; Waddington et al., 2007).

97 Despite the large spatial coverage of radar data across Antarctica, information on
98 dated IRHs is limited over much of the WAIS. This is partly due to the restricted availability
99 of deep ice cores, the multitude of radar-system families operating at varying frequencies and
100 using different post-processing methods to generate the radar data, and the challenge in
101 tracing deep continuous IRHs, particularly through areas of high strain rate (i.e. at the onset
102 of fast-flowing tributaries). Nonetheless, previous studies over the WAIS have used IRHs for
103 the direct purpose of linking major deep ice cores together (Koutnik et al., 2016; Neumann et
104 al., 2008), while others have used a wider, catchment-scale approach to constrain information
105 on past accumulation rates and ice-flow reconfiguration. Such studies have ranged across the
106 central WAIS (Jacobel and Welch, 2005; Muldoon et al., 2018; Siegert and Payne, 2004), or
107 focused on specific sub-regions, e.g., Siple Dome (Jacobel et al., 1996), Kamb Ice Stream
108 (Catania et al., 2006; Holschuh et al., 2018) and Thwaites Glacier (Muldoon et al., 2018).

109
110 Over PIG, Karlsson et al. (2014) identified two IRHs spanning much of the slow-
111 flowing parts of the catchment, which they roughly dated to 5.3-6.2 and 8.6-13.4 ka. More
112 recently, Ashmore et al. (2020) recovered three IRHs ranging across Institute and Möller Ice
113 Streams and crossing the Institute/PIG divide which they broadly dated at 1.9-3.2, 3.5-6.0,
114 and 4.6-8.1 ka. They demonstrated a correspondence between their IRH package and the
115 IRHs previously identified by Karlsson et al. (2014) and Siegert et al. (2005), suggesting that
116 a spatially-extensive network of IRHs may span much of the WAIS.

117
118 Here, we build on previous studies to present a spatially-extensive, dated-
119 radiostratigraphy of PIG. We use ice-penetrating radar data collected from two airborne
120 platforms to trace four IRHs throughout PIG. We use a published ice-core chronology as well
121 as a steady-state vertical-strain model to date these IRHs, and show that they span much of
122 the late Pleistocene and Holocene. We first discuss the specifications of the radar systems and
123 their respective uncertainties, and then describe the methods used to assign ages to each of
124 our four IRHs. We present the dated age-depth stratigraphy of the catchment and make
125 inferences for the rest of WAIS by comparing our recent findings to other age-depth studies.
126 Finally, we investigate the link between sulphate activity in the WAIS Divide ice-core record
127 and the depth of our upper three IRHs, and discuss to potential to recover records of older
128 (i.e. pre-LGM) ice in the region using currently available radar datasets.

2 Data Sets and Methods

2.1 Data

The principal data used in this study were acquired during two large-scale airborne radar surveys of West Antarctica.

The first of these was acquired over the 2004-05 austral season, when PIG's 175 000 km² catchment was surveyed extensively using the British Antarctic Survey's Polarimetric Airborne Survey INstrument (PASIN) system (Vaughan et al., 2006). This survey, hereafter termed "PIG-PASIN", acquired ~35 000 line-km of airborne radar data across the region (Figure 1). Data were collected with two interleaved radar modes. The first was a deep-sounding, 150 MHz centre-frequency, 4- μ s, 10 MHz chirp mode, which has been used previously to identify and trace the bed (Vaughan et al., 2006) and some IRHs (Karlsson et al., 2009; 2014). The second was a 150 MHz, 0.1- μ s pulse mode designed to image shallow IRHs but from which we are also able to recover IRHs deeper (~2 km, see Figure 2a) in the ice column. Over much of the region survey flight lines form 30 km spaced grids that contain multiple crossovers, ensuring consistency when tracing IRHs across neighbouring lines (Figure 1). Following techniques outlined in Ashmore et al. (2020), here we used both modes of PASIN interchangeably during our IRH-tracing procedures (see 2.2). For the purposes of linking our stratigraphy further across the WAIS, we also refer to further PASIN-acquired data from a survey of Institute and Möller Ice Streams undertaken in 2010-11 (hereafter "IMAFI-PASIN"), which provided tie-lines connecting PIG with its neighbouring basins (Figure 1; see Ashmore et al., 2020, and references therein, for further details).

The second survey was conducted in 2016 and 2018 by NASA's Operation IceBridge (OIB) mission, and yielded ~3 000 line-km of airborne radar data over PIG, Institute and Möller Ice Streams and Thwaites Glacier (Figure 1). The system deployed by the Center for Remote Sensing of Ice Sheets (CReSIS) was the Multichannel Coherent Radar Depth Sounder 2 (MCoRDS2) with a 190 MHz centre frequency and 50 MHz bandwidth. We used the CReSIS L1B standard products, produced with pulse compression, focused-SAR processing and along-track motion compensation. More information on the radar system and processing is given by CReSIS (2016). Critically for this study, one of the OIB flight tracks over PIG also flew over the WAIS Divide Ice Core (79.48°S, 112.11°W; hereafter referred to as WD2014) (Figure 1), making it possible to assign relatively unambiguous dates to the traced IRHs.

More details on each of the radar systems are provided in Table 1. For the purposes of increasing IRH traceability on the PIG-PASIN data, we quadratically detrended each radar trace, normalised each pixel in a moving vertical window, and then applied a 10-trace horizontal average to reduce incoherent noise (after Ashmore et al., 2020). For both the PIG-PASIN and the OIB-MCoRDS2 data, we removed the air-to-ice two-way travel time and shifted the surface elevation to time zero, prior to exporting the data to standard 2-D SEG-Y format for data interpretation.

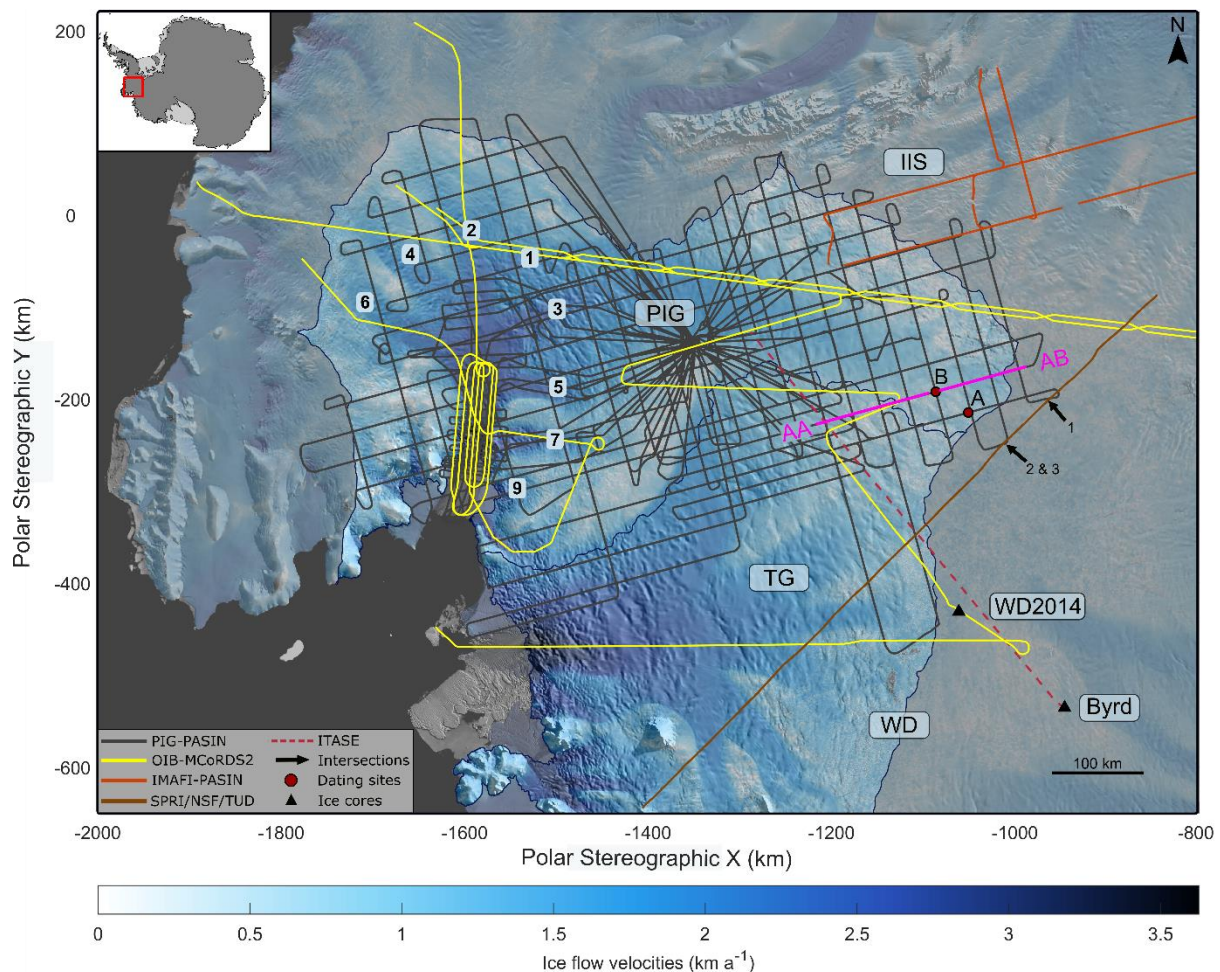


Figure 1. Map of study area with the data sets and key locations mentioned in this paper. The inset in top left corner shows the region of interest (red box). Airborne survey lines included in this study: PIG-PASIN (grey), OIB-MCoRDS2 (yellow), IMAFI-PASIN transects flown over Institute Ice Stream (ISS) and intersecting the PIG catchment (orange), SPRI/NSF/TUD line (brown), overlaid on top of ice flow velocities from Rignot et al. (2017) and MODIS Mosaic of Antarctica (Scambos et al., 2007). Also included is the long, ITASE GPR-transect (dashed red) through which the 17.5 ± 0.5 ka layer from Jacobel and Welch (2005) was traced. The numbers shown over PIG's trunk represent the eight fast-flowing tributaries (1-7, 9) mentioned in this paper. The WAIS Divide (WD2014) and Byrd ice cores are represented by the two black triangles, and the black arrows represent the three intersections between the SPRI/NSF/TUD-traced IRHs and this study. The two red circles show the two sites (Site A and B) where the 1-D age-depth model was used. The AA-AB segment (magenta) shows a subset of the control line where IRHs were first identified over PIG-PASIN (see Figure 2). The Western Divide is shown as WD on the map. The ICESat IMBIE basins of Pine Island Glacier (PIG) and Thwaites Glacier (TG) (Zwally et al., 2012) are annotated on the map and delimited by the blue outline lines.

2.2 IRH-Tracing Workflow

We conducted all IRH-tracing in the Schlumberger Petrel[®] 3-D seismic software using a semi-automated tracing algorithm that uses an adjustable window to track the local maxima of received reflected power between traces.

We initiated our workflow on the PIG-PASIN dataset as it is the most spatially-extensive survey of the PIG catchment. From a “control line” crossing the ice divides between PIG, Thwaites Glacier and Institute Ice Stream (Figure 1), in which clearly-visible englacial stratigraphy is ubiquitous in both chirp- and pulse-mode data, we identified four prominent IRHs that we term R1-4 (Figure 2). The upper three IRHs (R1-3) were chosen on

the basis of high spatial continuity, high signal-to-noise ratio (SNR), and as being analogous to “IRH packages” traced over part of PIG by Karlsson et al. (2014) and through IMAFI-PASIN radar profiles by Ashmore et al. (2020). All four IRHs occur in the middle part of the ice column where IRHs are likely resulting from contrasts in acidity from past volcanic eruptions (Gow and Williamson, 1971; Millar, 1981; 1982), rather than the result of density variations occurring primarily at the near-surface (Gow, 1970; Clough, 1977; Moore, 1988) or orientation of anisotropic material due to ice foliation in the basal zone (Fujita et al, 1999; Harrison, 1973); and thus can be assumed to be isochronous (Siegert et al., 1998; Whillans, 1976).

Expanding out from the control line, we progressively traced and mapped IRHs across the catchment using IRH intersections at each crossover as calibration points. This ensured reliability in our reflection tracing as the software is capable of detecting intersecting IRHs at the crossover with orthogonal radar lines. Since our tracing strategy was based on reflector echo strength and continuity, the reflection tracing was terminated when it was no longer possible to distinguish visually between adjacent reflections, either as a result of similar brightness levels or a loss in continuity. This was particularly common in areas of steep bed topography causing IRHs to dip significantly, or where enhanced ice-flow speeds disrupted IRH continuity, notably into the main flow features of PIG’s northern catchment. In some places, IRHs faded without such clear topography/flow-induced reasons, likely due to the attenuation of the radar signal with depth or the type of processing used (Holschuh et al., 2014). In some locations more distant from the upper PIG catchment (i.e. southward of tributary 6; Figure 1), extensive englacial layering was visible in radar profiles but, due to a dearth of connecting lines and crossovers, we could not, with confidence, identify R1-4.

When tracing between crossovers, we relied upon the distinctiveness of our IRHs. At the vertical resolution of PASIN, R1 and R2 manifest as single-amplitude peaks, with R2 representing a particularly bright reflector widely visible across our radar data (Figure 2, Figure S1). R3 consists of the shallowest of a series of closely-spaced bright horizons, often manifested as a couplet (zoomed inset in Figure 2, Figure S1), and previously identified by Karlsson et al. (2014; their “Layer 2”) and Ashmore et al. (2020; their “H3”). The lowermost IRH, R4, forms the upper part of a band of bright reflectors visible at the intersection with the 17.5 ± 0.5 ka layer widely imaged on radar data from the International Trans-Antarctic Scientific Expedition (ITASE) connecting the PIG catchment with the Byrd Ice Core chronology (Hammer et al., 1997; Jacobel and Welch, 2005) (Figure 1-2, Figure S1).

Once R1-4 were traced through the PIG-PASIN survey, we looked for the same IRHs on the OIB-MCoRDS2 data using available crossovers between each survey (Figure 1 & 3). We found R2-3 to be equally distinguishable in OIB-MCoRDS2 profiles, with R2 representing a particularly bright reflector similar to that on PIG-PASIN, whilst R3 also formed the shallower part of an easily distinguishable couplet. We did not recover R1 independently on the OIB-MCoRDS2 profile crossing the WAIS Divide ice-core and used intersections with PIG-PASIN to trace it across to Institute Ice Stream catchment. Similarly, we used several intersections with the 17.5 ± 0.5 ka layer from Jacobel and Welch (2005) in and around the WD2014 site to recover R4 in the OIB-MCoRDS2 data (Figure 1 & 3).

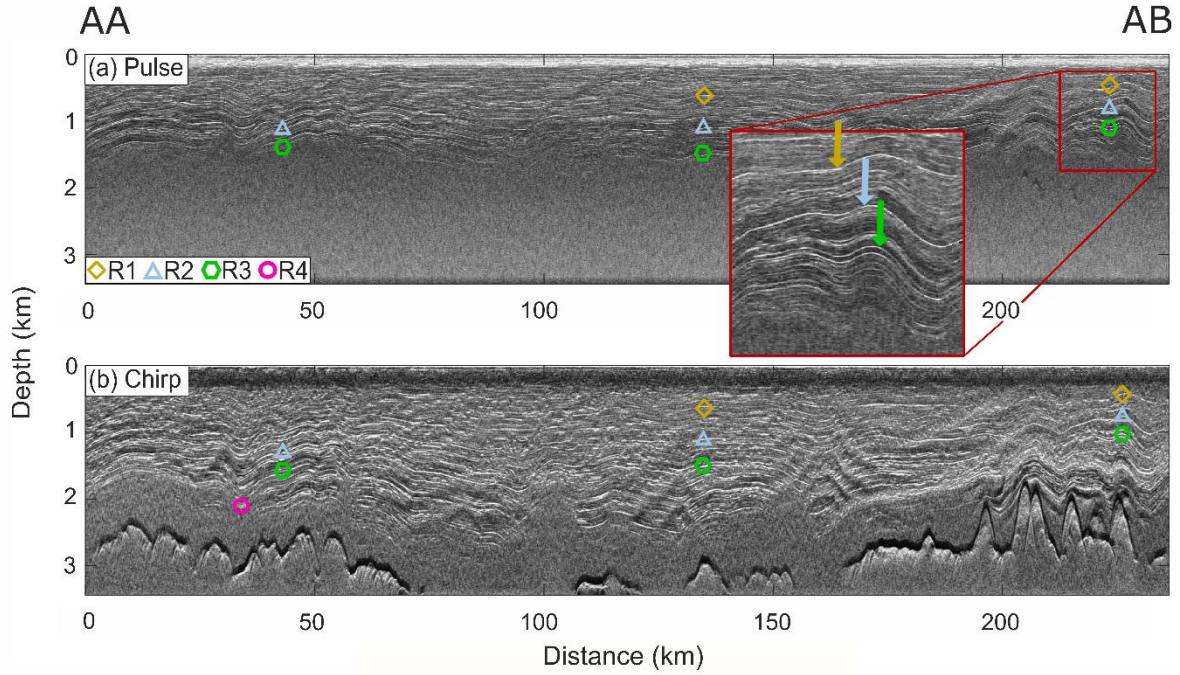


Figure 2. Subset of the control line with the unmodulated pulse (a) and chirp (b) modes from the PIG-PASIN survey along transect AA– AB (see Figure 1). Traced IRHs are marked as per the legend on panel (a). The zoomed inset on the pulse radargram shows the characteristics of R1-3 in more detail, with the colour of the arrows corresponding to the legend in (a).

It is worth noting that the OIB-MCoRDS2 data were acquired 12-14 years later than the PIG-PASIN survey, and so the same IRHs will, in principle, lie slightly lower in the ice column. However, considering a present-day mean accumulation rate of $\sim 0.30\text{-}0.35 \text{ m a}^{-1}$ (metres of ice equivalent per year) at the intersection between the two surveys, the maximum change in IRH depth is $< 5 \text{ m}$. This is well within the bounds of the total depth uncertainty calculated for each radar system (see 2.3) and does not affect the pattern of englacial layering or the identification of our IRHs across the different surveys. Crossover analysis at key intersections on the airborne radar data showed that the mean depth difference for R1-4 fall within the uncertainty range of all surveys (Figure S2, Table S1-2) (see 2.3). At 10 intersections on PIG-PASIN, the mean depth difference for R1-4 is $< 6 \text{ m}$. Similarly, mean depth difference for R2-3 at 11 intersections between PIG-PASIN and OIB-MCoRDS2 is 14 m and 29 m respectively, and $< 18 \text{ m}$ at five intersections between R4 on OIB-MCoRDS2 and the $17.5 \pm 0.5 \text{ ka}$ from Jacobel and Welch (2005) (Figure S2, Table S2).

With our objective being to produce an age-depth radiostratigraphy across PIG, we converted all IRHs traced above in the time domain (t_{IRH}) to depth (d_{IRH}) using

$$d_{IRH} = \frac{v_{ice} t_{IRH}}{2} + Z_f, \quad (1)$$

where $v_{ice} = 168.5 \text{ m } \mu\text{s}^{-1}$ is the speed of electromagnetic waves through ice (c.f. Fujita et al., 2000) and $Z_f = 10 \text{ m}$ is a spatially-invariant firm correction, appropriate for West Antarctica (Ashmore et al., 2020). All our depth measurements are given in metres below the surface. We then calculated IRH depth as a function of ice thickness using the ice-thickness measurement from each respective radar mission, and complemented these with ice-thickness

measurements from BedMachine (Morlighem et al., 2020) in places where the radar did not sound the bed.

2.3 Catchment-Wide Depth Uncertainties

To assess the accuracy of our IRH depths at the catchment scale, we consider the uncertainties associated with the imaging of IRHs with ice-penetrating-radar. These uncertainties primarily depend on three factors: variations in the speed of electromagnetic wave (EM) through the ice, firn-density correction, and the radar system's range precision (Cavitte et al., 2016) (Text S1).

The maximum uncertainty arising from selecting an EM value ranging between 168 and 169.5 m μs^{-1} is 16 m on the maximum depth of the deepest reflection on PIG-PASIN and 14 m on OIB-MCoRDS2. The uncertainty associated with the firn correction is ± 3 m, owing to minor variations in firn densification across the catchment (Ashmore et al., 2020) (Text S1). The precision of IRH depth estimates also depends on the range accuracy, $\sigma(r^*)$, of the radar system, which refers to how accurately changes can be located in 3-D space (Cavitte et al., 2016; King, 2020). This is a combination of the SNR of each IRH and the range resolution, Δr , of the radar system, which is mainly a function of sampling frequency, bandwidth, source wavelets, and the type of post-processing applied. The range resolution for each system, from coarser to finer is: PASIN chirp (12.89 m), PASIN pulse (8.42 m), and MCoRDS2 (2.58 m) (Table 1, Text S1).

Table 1. Characteristics and resolution of the two airborne radar systems used in this study. Note that for the PASIN system, we provide values for both the chirp- and pulse-acquisition mode in the bandwidth/pulse width column, as well as in the vertical resolution column. The vertical resolution of the chirped systems was calculated as per CReSIS (2016) using a scaling factor 'k' which accounts for resolution degradation due to receiver characteristics and processing (see Equation S1).

System	Platform	Centre Frequency	Bandwidth / Pulse Width	Vertical Sampling Frequency	Vertical Resolution	Horizontal Sampling Distance
PASIN	Twin Otter	150 MHz	10 MHz / 100 ns	22 MHz	12.89 / 8.42 m	45 m
MCoRDS2	DC8	190 MHz	50 MHz	150 MHz	2.58 m	14 m

We undertook an empirical error analysis to calculate the maximum uncertainty associated with the deepest IRH by calculating the root-mean-square error of the depth uncertainties from EM wave through the ice, the firn correction, and the radar range accuracy. We obtained a combined maximum uncertainty of ± 17 m and attached this uncertainty to all IRHs traced on the PIG-PASIN data (Text S1). Similarly, we estimated a combined maximum uncertainty of ± 14 m on the OIB-MCoRDS2 data (Text S1). Given that this uncertainty represents the maximum uncertainty on the deepest IRH over our entire dataset, we also calculate IRH-specific uncertainties at the ice-core site (see 2.4.1).

2.4 Age-Depth Attribution

To estimate the absolute age of our IRHs, we employ two primary dating methods: we use (a) the WAIS Divide ice-core chronology to provide a direct age to our three deepest IRHs, namely R2-4; and (b) the Dansgaard-Johnsen 1-D model to independently compare the ages calculated at the ice core and to provide an approximate age range to our shallowest IRH, R1. Once dated, we also compared the ages and depths of R1-3 with dated IRHs traced

across PIG (Siegert and Payne, 2004; Karlsson et al., 2014) and Institute and Möller Ice Streams (Ashmore et al., 2020); as well as the age and depth of R4 with the 17.5 ± 0.5 ka layer dated using the Byrd ice-core chronology (Hammer et al., 1997) and traced across the WAIS (Jacobel and Welch, 2005). Finally, we also compare the depth and age of our upper three IRHs with sulphate concentrations from the WD2014 ice-core record (Cole-Dai, 2014; McConnell et al., 2017).

2.4.1 Connection to the WAIS Divide ice-core chronology

We used the 2016 OIB-MCoRDS2 data linking central PIG to the WD2014 site to date IRHs across PIG relative to the ice-core chronology, where annual-layer counting goes back to the last ~31 ka BP (Buizert et al., 2015; Sigl et al., 2016). We take the recorded depth at the ice core which most-closely matches our IRH depth at WD2014, and calculate the upper and lower age bounds using the radar depth and ice-core uncertainties. Following MacGregor et al. (2015), the age uncertainty (Δa_{comb}) associated with each IRH is the root-mean-square combination of the age uncertainty associated with the unweighted mean IRH depth at the ice core ($\Delta a_{\Delta depth}$) and the age uncertainty associated with the ice core at the IRH depth (Δa_{core}), following

$$\Delta a_{comb} = \sqrt{\Delta a_{\Delta depth}^2 + \Delta a_{core}^2}, \quad (2)$$

where (Δa_{core}) is a function of the age of the individual IRH at the ice core site (Sigl et al., 2016) and the published uncertainty associated with the ice core age (1% and 3% for ages ranging between 0-15 ka and 15-31 ka BP respectively; Sigl et al., 2016), while ($\Delta a_{\Delta depth}$) is a function of the depth uncertainty of each IRH at the ice-core site. Since the uncertainty in the electromagnetic wave through the ice increases with depth, using the maximum uncertainty calculated on the deepest IRH to calculate $\Delta depth$ at a catchment scale (see 2.3) would result in less accurate age uncertainties at the ice core. We have therefore calculated a depth uncertainty for each individual IRH at the ice core, and undertook the same empirical error analysis to calculate $\Delta depth$ at WD2014. This resulted in IRH-specific radar depth uncertainties which we used to calculate the age uncertainty for each IRH at WD2014, as per Equation 2.

Whilst Δa_{comb} represents the combined maximum uncertainty from the radar and the ice-core chronology, we found that our IRHs are systematically lower in the ice column compared with strong peaks in acidity concentrations at WD2014 matching closely the age and depth of our IRHs and which we can assume to be the likely cause of our IRHs (see 4.2). To account for this offset in ages between the IRHs and the strong sulphate peaks observed at WD2014, we calculated a total age uncertainty (Δa_{total} , Table 3) which represents the maximum age difference between our IRHs and the sulphate peaks at the ice core. This was obtained by adding a systematic factor of 0.22 ka to Δa_{comb} , which represents the total age difference between the maximum IRH age calculated using Δa_{comb} and the age of the strong sulphate peaks (see 4.2). We provide the total uncertainty values in Table 3 and Section 3.2.

2.4.2 Age-depth modelling

To provide an independent validation of our ice-core derived IRH ages, we also applied the Dansgaard and Johnsen (1969) 1-D vertical ice-strain rate model to derive approximate dating of the IRHs traced over the central PIG catchment. This model has been

used previously to date IRHs across West Antarctica (Corr and Vaughan, 2008; Karlsson et al., 2012; 2014; Ashmore et al., 2020), assess divide migration (Waddington et al., 2005), and calculate past accumulation rates at or near ice divides (Siegert and Payne, 2004; Jacobel and Welch, 2005). We chose the Dansgaard–Johnsen model here for its simplicity and as it allows us to test the effect of ice deformation on the ages of our IRHs. However, we note that other alternatives exist such as the Nye (Nye, 1957) and Lliboutry (Lliboutry, 1979) models, or the more developed quasi-Nye model (MacGregor et al., 2015).

Under the assumption that the ice sheet is, and has been, in steady state, close to an ice divide, the Dansgaard-Johnsen model gives

$$t = \frac{2H-h}{2a} \ln \left(\frac{2H-h}{2z-h} \right), \quad h \leq z \leq H, \quad (3)$$

where t (ka; thousand years) is the age of an IRH, H (m) is the ice thickness (assumed constant in time), h (m) is the thickness of the basal shear layer, a (in m a^{-1} ice-equivalent) is the average accumulation rate since deposition of the IRH, and z (m) is the elevation of the IRH above the bed (Dansgaard and Johnsen, 1969).

For this model, several assumptions are made: (a) negligible horizontal velocity component; (b) time-averaged accumulation rates and no temporal change in accumulation patterns; (c) constant ice deformation from the surface to some depth, h , below which vertical strain rate is assumed to decrease linearly towards the bed. Considering the above, we initiated the model on the PIG-PASIN data at two sites (A and B in Figure 1) located ~50 km from the ice divide where horizontal ice flow is minimal ($< 3 \text{ m a}^{-1}$), the ice is thick ($> 3 \text{ km}$) and the bed relatively flat. Site A (80.15°S , 101.56°W) was selected due to its relative proximity within PIG to WD2014 (~215 km). At this site, R1-3 were traced, as well as R4. This provided us with initial constraints for age-depth estimates for the upper IRHs (namely R1-3), and allowed us to evaluate the model results based on the approximate known age of R4. To ensure representativeness, however, we also selected a second site, Site B (79.87°S , 100.03°W), where R1-3 were traced but not R4.

We based our estimates for a in the equation on advection-corrected accumulation rates from the WD2014 ice core (Fudge et al., 2016) for each IRH R1-4, and with current accumulation estimates to correct for any elevation-dependent change in accumulation between the WD2014 site and our PIG Sites A and B. Tentatively treating our R1-3 as broadly equivalent to three of Siegert and Payne's (2004) dated IRHs based on depth associations at three crossovers (see Text S2, Table S3), we derived mean advection-corrected accumulation rates at WD2014 for each reference age: $0.247 \pm 0.062 \text{ m a}^{-1}$ (3 ka BP, with BP defined as years before 1950 CE), $0.248 \pm 0.062 \text{ m a}^{-1}$ (5 ka BP), and $0.243 \pm 0.061 \text{ m a}^{-1}$ (7 ka BP), as well as a rate of $0.226 \pm 0.051 \text{ m a}^{-1}$ (17.5 ka BP) based on the intersection with Jacobel and Welch (2005). The errors correspond to uncertainties in the firn-densification model used by Fudge et al. (2016). These provide us with estimates of what would be required to reproduce each layer if accumulation had remained constant between the time of the deposition of the layer and the present at WD2014. Under the assumption that spatial accumulation patterns have not changed during the Holocene over the WAIS (Koutnik et al., 2016; Neumann et al., 2008; Siegert and Payne, 2004), and considering that accumulation rates at the ice-core are generally smaller than at Site A and B (Table S4), we use modern accumulation rates from modelled and observational data to calculate the regional difference between accumulation at WD2014 and our Sites A and B. The four

sources of accumulation data used here are: (a) surface mass balance (SMB) estimates for the period 1979-2015 using the Modèle Atmosphérique Régional (MAR, Version 3.6.4; Agosta et al., 2017); (b) SMB estimates for the period 1979- 2018 from the Regional Atmospheric Climate Model 2 (RACMO2; van Wessem et al., 2018); (c) accumulation rates interpolated from ground measurements and AMSR-E polarisation (Arthern et al., 2006; hereafter referred to as ART06); and (d) a combination of catchment-wide, snow and accumulation radar measurements obtained in 2009-11 from ultra-wideband airborne platforms and intersecting a series of shallow ice cores (Medley et al., 2014), combined with a set of GPR tracks acquired in 2002-04 over the Western Divide (Neumann et al., 2008) (hereafter referred to as MED14) (Text S2). From these data sets, we calculate a percentage of change between WD2014 and Site A-B and apply this to the mean advection-corrected rates calculated at WAIS Divide for R1-4 (Table S4). Together, these provided us with a range of realistic values of a for each IRH at Site A-B to use as input into the 1-D model.

The thickness of the basal shear layer, h , is largely unknown as it is dependent on accurate knowledge of the bed topography and temperature of the ice (Neumann et al., 2008). Previous studies have used a value of $h = 400\text{ m}$ for Greenland and West Antarctica (Fahnestock et al., 2001b; Siegert and Payne, 2004; Jacobel and Welch, 2005; Karlsson et al., 2012), whilst Karlsson et al. (2014) and Ashmore et al. (2020) explored the effects of fuller ranges of $100\text{ m} \leq h \leq 1200\text{ m}$. We refined this range to $0.2H \leq h \leq 0.3H$ (Neumann et al., 2008), rounding to the nearest 100, hence investigating the effect of h ranging from 700 to 1100 m at both sites (Text S2). We note, however, that large uncertainties in basal deformation at WD2014 (Cuffey et al., 2016; Fudge et al., 2019) could result in h values being smaller than 20% of the ice thickness and thus lead to an overestimation of our ages (see Text S2).

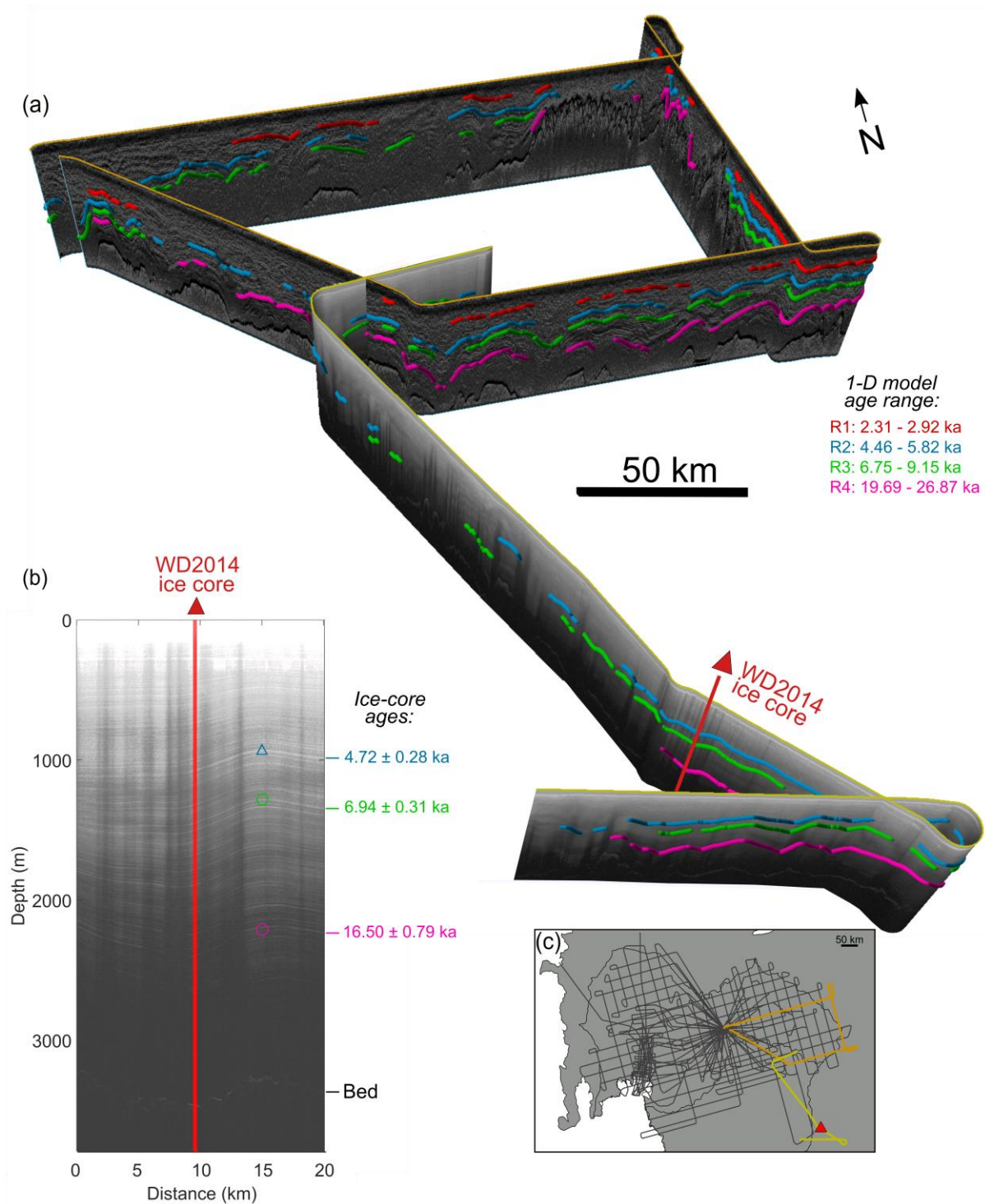


Figure 3. (a) Intersecting radar profiles from PIG-PASIN and OIB-MCoRDS2 with IRHs R1 (red), R2 (blue), R3 (green) and R4 (pink) traced along radargrams. The age range shown on the PIG-PASIN profile in the top right corner are from the 1-D model for R1-4 (see 3.2). (b) Englacial layering on the OIB-MCoRDS2 radar profile where it intersects the WD2014 ice core (red line), with ages and total age uncertainties for R2-4 inferred from the ice-core chronology (see 3.2) shown on the right-hand side. (c) Inset showing the PIG-PASIN (orange line) and OIB-MCoRDS2 (yellow line) profiles in (a) and the full PIG-PASIN radar flight lines shown in grey in the background, as well as the position of the WD2014 ice core (red triangle).

3 Results

3.1 Englacial Stratigraphy

We successfully traced four IRHs R1-4 across a large proportion of the PIG catchment, including in areas where annual velocities reach up to $\sim 350 \text{ m a}^{-1}$ (Figure 4). The most extensive IRH traced in our study is R2, closely followed by R3 (Figure 4), with mean depths across the catchment of 1175 and 1463 m respectively (Table 2). The shallowest IRH, R1, was located on average at $\sim 30\%$ of the ice depth, whilst the deepest, R4, was on average found at $\sim 68\%$ depth (Table 2).

Table 2. Summary statistics for each IRH traced throughout the PIG-PASIN and OIB-MCoRDS2 surveys. We provide these for both depth below the surface and depth as a fraction of ice thickness. “ 1σ ” refers to one standard deviation, “Range” refers to the minimum and maximum values, and “IQ Range” refers to the interquartile range (25th and 75th percentile). A maximum uncertainty of $\pm 17 \text{ m}$ is assumed here.

	<i>IRH depth statistics</i>							
	<i>Depth below the surface (m)</i>				<i>Depth as fraction of ice thickness</i>			
	Mean	1σ	Range	IQ Range	Mean	1σ	Range	IQ Range
R1	722	191	204 - 1302	623 - 873	0.30	0.10	0.12 – 0.63	0.22 – 0.36
R2	1175	240	304 - 2014	1069 - 1347	0.46	0.09	0.21 – 0.82	0.40 – 0.52
R3	1463	298	650 - 2486	1324 - 1650	0.54	0.08	0.29 – 0.82	0.48 – 0.60
R4	1929	257	697 - 2640	1799 - 2080	0.68	0.05	0.42 – 0.92	0.66 – 0.71

The traceability of R1-3 does not vary greatly and is primarily constrained by topography (Figure 4a-c). By contrast, R4 was only detected across the upper Thwaites/PIG (Figure 4d), even though it has previously been detected much further north into the PIG basin in the ITASE survey (Jacobel and Welch, 2005), likely due to the different frequency range used by the two radar systems. We come back to this point in Section 4.1. We were also able to trace R1-3 in the upper parts of the Institute and Möller ice-stream catchment, and R2-4 in the upper parts of the Thwaites catchment toward the WD2014 site (Figure 4). The traced IRHs are generally deeper southward of the onset of PIG tributaries 7 & 9 and at the centre of the PIG catchment, and relatively shallow at its southern margin and at the divides with Thwaites Glacier and Institute Ice Stream (Figure 4e-h). We were unable to identify the IRHs in several locations, mainly north of the main trunk of PIG near the Hudson Mountains range and west of tributary 6 (Figure 4a). We were also unable to detect continuous IRHs in any PIG-PASIN profiles traversing the main trunk and tributaries of Thwaites Glacier, nor those that cover the main trunk and fast-flowing tributaries of PIG (Figure 4).

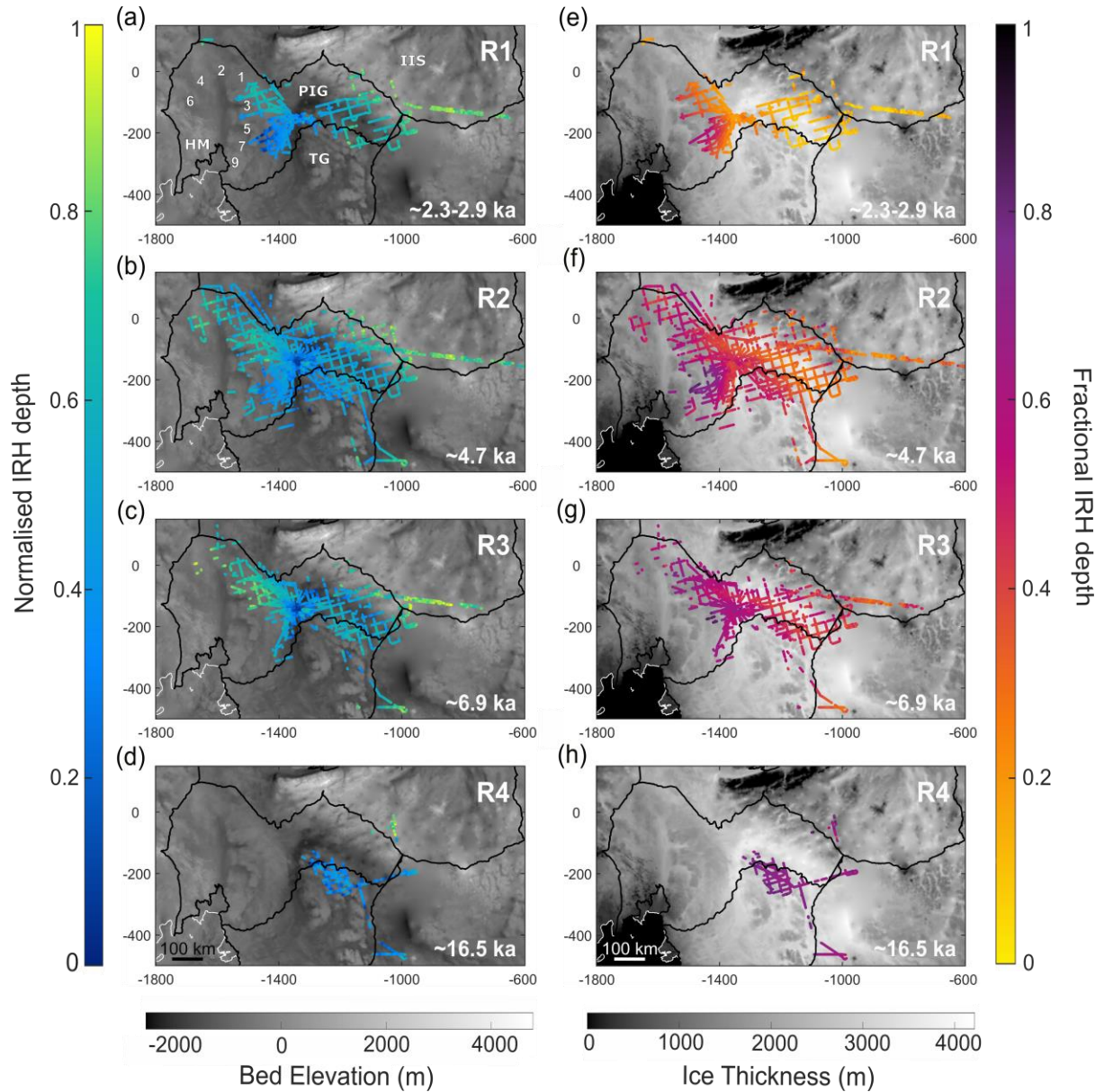


Figure 4. Normalised (a-d) and fractional (e-h) depth for the four IRHs traced over the PIG-PASIN and OIB-MCoRDS2 data from shallowest to deepest. Also shown are the IRH ages (ka) (see 3.2) for R1 (age-range estimate from 1-D model) and R2-4 (ages from WD2014 ice-core intersection). For (a-d), lower (blue) values correspond to relatively deep IRH depths, higher (yellow) values correspond to shallow IRH depths. Background is bed elevation in metres (referenced to the WGS84 ellipsoid) from BedMachine (Morlighem et al., 2020). For (e-h), lower (yellow) values correspond to the shallowest IRHs, higher (purple) values correspond to the deepest IRHs. Background is ice thickness in metres from BedMachine (Morlighem et al., 2020). The white line is the Antarctic coast line. The numbers and annotations in (a) are the eight fast-flowing tributaries (1-7, 9) of Pine Island Glacier, the location of the Hudson Mountain Range (HM), and the ICESat IMBIE basins containing the Pine Island Glacier (PIG), Thwaites Glacier (TG) and Institute Ice Stream (ISS) (Zwally et al., 2012).

3.2 Age-depth Estimates

Having clearly identified R2-4 near the WD2014 site, we attempt to date these using the WD2014 chronology. The OIB-MCoRDS2 radar profile passes within ~ 1.2 km of the ice-core site, however the stable ice conditions in the area means that flow-induced disturbance on layer geometry is relatively limited (Laird et al., 2010). Following MacGregor et al.

(2015), we calculate the unweighted mean reflection depth within a distance of ± 250 m along transect from the trace that is closest to the ice-core site to obtain $\Delta a_{\Delta depth}$, resulting in mean depths at the ice core of 1060 ± 7 (R2), 1430 ± 9 (R3), and 2371 ± 14 m (R4) (Table 3). Considering the radar-depth and ice-core uncertainties (Equation 2), and to account for the age offset between our IRHs and the strong sulphate peaks at the ice core (see 2.4.1 and 4.2), we determined the age and associated age uncertainty for each IRH at WD2014 as: 4.72 ± 0.28 (R2), 6.94 ± 0.31 (R3), and 16.50 ± 0.79 ka (R4) (Table 3).

Table 3. IRH mean depths (m), ages (ka; in years before 2020 AD), and uncertainties (Δ) at the WD2014 site for R2-4. Column “ a (ka)” refers to the IRH age obtained from the radar-depth and the depth at the WD2014 ice core. Column “ Δa_{comb} ” refers to the combined age uncertainty from the radar and the ice-core chronology, whilst “ Δa_{total} ” refers to the maximum age uncertainty of our IRHs calculated from the age difference between our IRHs and the strong sulphate peaks at WD2014 (see 2.4.1, 4.2).

	<i>depth</i> (m)	$\Delta depth$ (\pm m)	<i>a</i> (ka)	$\Delta a_{\Delta depth}$ (\pm ka)	Δa_{core} (\pm ka)	Δa_{comb} (\pm ka)	Δa_{total} (\pm ka)
R2	1060	7	4.72	0.04	0.05	0.06	0.28
R3	1430	9	6.94	0.06	0.07	0.09	0.31
R4	2371	14	16.50	0.28	0.50	0.57	0.79

To compare the ages independently from the WD2014 chronology and provide an approximate age-range estimate for our shallowest isochrone R1, we use the 1-D model at Site A and B. The age estimates returned from the 1-D model at both sites are as follows: R1 (2.31-2.92), R2 (4.46-5.82), R3 (6.75-9.15), and R4 (19.69-26.87 ka) (Table 4).

Table 4. Modelled IRH age-range estimates (ka) returned from the 1-D steady-state model for varying accumulation datasets (see 2.4.2) and basal shear layer thickness (h , in metres) scenarios at Site A and B for IRHs R1-4 (see 2.4.2). Note that at Site B, R4 was not retrieved. The accumulation rates (m a^{-1}) used to obtain each IRH age estimate can be found in Table S4. We calculate an empirical error estimate of between ± 2 and 4% for each modelled age estimate based on the uncertainties in radar depth (± 17 m) and ice thickness (± 23 m, Vaughan et al., 2006).

		<i>Site A</i>			<i>Site B</i>		
		<i>h</i> = 700	<i>h</i> = 900	<i>h</i> = 1100	<i>h</i> = 700	<i>h</i> = 900	<i>h</i> = 1100
R1	MAR	2.84	2.85	2.86	2.89	2.90	2.92
	ART06	2.68	2.69	2.70	2.78	2.80	2.81
	RACMO2	2.36	2.37	2.38	2.32	2.33	2.34
	MED14	2.31	2.32	2.33	2.36	2.37	2.38
R2	MAR	5.72	5.77	5.82	5.55	5.61	5.67
	ART06	5.40	5.44	5.49	5.35	5.40	5.46
	RACMO2	4.75	4.79	4.84	4.46	4.50	4.55
	MED14	4.65	4.69	4.73	4.57	4.62	4.67
R3	MAR	8.88	9.01	9.15	8.41	8.54	8.69
	ART06	8.38	8.50	8.63	8.10	8.23	8.37
	RACMO2	7.38	7.48	7.60	6.75	6.86	6.98
	MED14	7.22	7.32	7.43	6.92	7.03	7.15
R4	MAR	24.22	25.40	26.87	-	-	-
	ART06	22.85	24.00	25.40	-	-	-
	RACMO2	20.13	21.10	22.32	-	-	-
	MED14	19.69	20.64	21.84	-	-	-

The ages calculated for R2-3 at WD2014 (Table 3) are within the upper and lower bounds of the modelled age-range estimates from the 1-D model (Table 4), with the MED14

and RACMO2 accumulation products best able to reproduce the ages at WD2014 to within < 10%. However, the returned age estimate for R4 at Site A, 19.69–26.87 ka, is 20 to 60% greater than the age of R4 at WD2014 (16.50 ± 0.79 ka) and that of Jacobel and Welch (2005) (17.5 ± 0.5 ka). We come back to these points in sections 4.1 and 4.3.

4 Discussion

4.1 IRH Comparison Across the WAIS

Karlsson et al. (2014) traced two distinctive IRHs through the middle ice depths across parts of the central PIG catchment using the same PIG-PASIN dataset as that used here, but only focusing on flight lines flown at constant elevation and only exploiting the data in its chirp mode. This earlier study highlighted the existence of a distinctive IRH package between an upper bound, “Layer 1”, approximately dated to 5.3–6.2 ka, and a lower bound “Layer 2”, approximately dated to 8.6–13.4 ka. Here, by additionally exploiting the full spatial extent of the PIG-PASIN dataset, the simultaneously-acquired pulse-mode PASIN data, and complementing these with recent OIB-MCoRDS2 data, we have expanded the reach of that earlier radiostratigraphy across the fuller PIG catchment, and across the ice divides into neighbouring regions, notably Thwaites Glacier and Institute Ice Stream. Direct comparison between both sets of results suggests that Karlsson et al.’s (2014) Layer 1 and 2 are equivalent to the IRHs traced in this study as R2 and R3, with a median difference ranging between 6 and 12 m, which is within the depth uncertainty of the IRHs (Figure S3).

Throughout the neighbouring Institute and Möller ice-stream catchments, Ashmore et al. (2020) also recently traced three prominent IRHs (H1–3), broadly dated at 1.9–3.2 (H1), 3.5–6.0 (H2), and 4.6–8.1 ka (H3), using the same 1-D model described here. They posited that their deeper two IRHs (namely H2–3) were also similar to Karlsson et al.’s (2014) Layers 1 and 2 (and hence are likely equivalent to our R2 and R3), but the association was untested with any direct crossovers. Here, we were able to trace our upper three IRHs R1–3 along an OIB-MCoRDS2 profile extending across the upper Institute Ice Stream catchment (Figure 4a–c), intersecting eight IMAFI-PASIN profiles in which H1–3 were traced. Across these intersections, the mean difference between OIB-MCoRDS2 R1–3 and IMAFI-PASIN H1–3 is 15 m, which is within the uncertainty bounds of the respective radar systems (± 14 m for OIB-MCoRDS2; ± 15 m for IMAFI-PASIN, Ashmore et al. (2020)), and hence provides additional evidence that we observe the same IRHs across both catchments. Two sets of parallel profiles, laterally offset by ~ 1.5 km, and acquired across the PIG/Institute Ice Stream divide in the PIG-PASIN and IMAFI-PASIN data sets (Figure 1), provide a further opportunity to confirm these equivalences with data from the same radar system. Only in three short sections of these transects could we compare our IRHs with those from the IMAFI-PASIN study (inset Figure S3a); in these locations, we could not identify R1 and R3. Nevertheless, at two intersections (black arrows in inset on Figure S3a), the respective depths for PIG-PASIN R2 and IMAFI-PASIN H2 were 794 and 797 m at Intersection 1 and 776 and 778 m at Intersection 2 respectively, which is remarkably close considering ice thickness in this area exceeds 2 km. This, alongside the crossovers on the OIB-MCoRDS2 data, gives us high confidence that our R2, Ashmore et al.’s (2020) H2, and therefore Karlsson et al.’s (2014) Layer 1, all represent the same internal marker in the ice. This study, by using additional data that allowed direct dating at the WD2014 site, is therefore able to ascribe

more accurate and precise ages to the IRH package ranging across PIG and Institute and Möller Ice Streams of 4.72 ± 0.28 ka (Layer 1/H2/R2) and 6.94 ± 0.31 ka (Layer 2/H3/R3) respectively based on the WD2014 ice-core chronology.

We also note that all three studies identify R2 as their most spatially-extensive IRH, indicating the presence of a particularly ubiquitous isochrone, similar in age to a 4.72 ± 0.24 ka isochrone detected and also extensively mapped elsewhere across central West Antarctica (Muldoon et al., 2018). Whilst we were not able to provide a more refined age to our shallowest IRH, R1, from direct intersection the WD2014 ice-core, the 1-D model returned an age-range estimate (2.31–2.92 ka) that is in broad agreement with that of Ashmore et al. (2020) (1.9–3.2 ka; their H1) and Siegert and Payne (2004) (3.10 ± 0.16 ka; their L07). Together, these studies demonstrate considerable promise for unifying an age-depth stratigraphy across the WAIS back to at least ~ 7 ka, while tying our IRHs to the WAIS Divide ice-core has yielded more accurate, and younger, ages, for the isochrones detected across PIG and, by extension, Institute and Möller Ice Streams.

The age assigned to R4 at WD2014 (16.50 ± 0.79 ka) is slightly younger than the 17.5 ± 0.5 ka layer tied by Jacobel and Welch (2005) to the Byrd Ice Core (Hammer et al., 1997), although there is an overlap of 0.29 ka when fully accounting for the age uncertainties. We offer two potential explanations for this disparity. Firstly, the low-frequency ground-radar system used as part of the ITASE survey has a much longer wavelength than the high-frequency airborne systems used here, meaning that the 17.5 ± 0.5 ka layer appears as a single-amplitude peak measuring tens of meters in thickness (c.f. Jacobel and Welch, 2005), whereas the shorter-wavelength on the airborne radars allows for the delineation of individual peaks, thus resolving the strong singular reflector from Jacobel and Welch (2005) as a series of closely spaced reflectors. As a result, when attempting to connect the ITASE profile with the airborne radar data, it is likely that the closest bright reflector identified on the airborne radar forms the upper part of the wider reflector imaged by Jacobel and Welch (2005), thus leading to younger ages at the intersection with the WAIS Divide ice core. Secondly, the uncertainties in the radar data at the intersection between OIB-MCoRDS2 (± 14 m) and Jacobel and Welch's (2005) profile (± 10 m) increase the chance to misinterpret the correct position of the 17.5 ka layer over the airborne data, although we show in Table S2 that the mean depth difference between R4 and Jacobel and Welch's (2005) layer is < 18 m, which is within the uncertainty range of both studies. Whilst these points are relevant when comparing the ages of R4 at WD2014 with the age of Jacobel and Welch's (2005) layer, it is worth mentioning that the exact age and depth of the strong reflector at WD2014 are known from electrical conductivity and chemistry measurements. At the ice core, this layer is characterised by 9 distinctive peaks ranging in depths between 2420 m and 2427 m and dated at 17.75 ± 0.19 ka (McConnell et al., 2017; Sigl et al., 2016), a full 35 m below the depth of R4 at WD2014. Even taking into account the maximum depth of our IRH along the ± 250 m transect (2378 ± 14 m; see 3.1), R4 is still found 28 m above the depth of the 17.75 ± 0.19 ka at WD2014. Considering all the above, it is likely that R4 is not the same layer as the strong volcanic layer dated at 17.75 ± 0.19 ka at WD2014 (McConnel et al., 2017), but rather forms the upper part of the wide reflector imaged by Jacobel and Welch (2005) in the ground-radar data.

4.2 Linkage with the WAIS Divide Ice-Core Record

Whilst determining the cause of R4 remains ambiguous due to the limitations mentioned above, the existence of R2 and R3 offer an opportunity to link them directly to the

ice-core sulphate record at WD2014. High sulphate content from volcanic sulphuric acid is known to correspond to high acidity levels in englacial layers in ice cores (Castellano et al., 2005; Gow and Williamson, 1971; Hammer et al., 1997; Millar, 1982) and, because the radar is sensitive to acidity contrasts (Fujita et al., 1999; Millar, 1981), we can attempt to link the sulphate record at the ice core with our IRH stratigraphy. Figure S4 shows the presence of three large peaks in sulphate concentration at the WD2014 ice core which are particularly close in age and depth to IRHs R2-3 traced on the OIB-MCoRDS2 profile near WD2014. In particular, a layer dated at 4.94 ka (depth: 1099 m) contains sulphate concentrations that are unmatched (405 $\mu\text{g/kg}$) for much of the core up until a depth of ~ 2400 m (equal to the last $\sim 18\,000$ years BP) (Figure S4). Even taking into account the entire profile, this layer contains the fourth largest amount of sulphate concentrations in the last $\sim 68\,000$ years BP. We also notice the presence of two closely-spaced peaks in the sulphate record which are dated at 7.25 ka (depth: 1475 m; sulphate concentration: 306 $\mu\text{g/kg}$) and 7.64 ka (depth: 1526 m; sulphate concentration: 271 $\mu\text{g/kg}$), corresponding to the 9th and 10th highest sulphate concentrations on record (Figure S4b). Not only do these ages match closely the age of R3 at the ice core, they also match the characteristics of R3, which is often found as a couplet across most of Pine Island, upper Thwaites, and Institute and Möller ice-stream catchments on the airborne radar data (Figure 2, S1). Additionally, the second largest peak on record before $\sim 18\,000$ years BP is found at a depth of 584 m and dated at 2.45 ka (sulphate concentration: 309 $\mu\text{g/kg}$), which falls within the modelled age-range estimate for R1 (2.31-2.92 ka) at Site A and B (Table 4, Figure S4a).

Whilst this offers us the opportunity to directly link our IRHs to the WAIS Divide record, we note that the depths of R2-3 at WD2014 are slightly shallower (R2: 1060 ± 7 m; R3: 1430 ± 9 m) than the sulphate peaks in Figure S4, resulting in slightly younger ages at the ice core. We cannot exclude the possibility that we traced a layer that is slightly above R2 and R3 at the ice-core, although this is unlikely as we base our tracing on depth intersections (Figure S2) and IRH characteristics (Figure S1). Even taking into account the maximum depth of R2-3 along our ± 250 m transect to account for the fact the OIB-MCoRDS2 line did not fly directly over the WD2014 site but instead ~ 1.2 km away (see 2.4.1), R2 (1069 ± 7 m) and R3 (1438 ± 9 m) would still be found 23 m and 28 m higher than the sulphate peaks at the ice core respectively. Whilst this is a relatively small disparity considering ice thickness in the area exceeds ~ 3.5 km and that we are effectively comparing airborne-radar data (meter-scale accuracy) with ice-core data (mm-scale accuracy), the reason for our IRHs not aligning more closely with the sulphate peaks remains unclear. One potential explanation could relate to the distance between our transect and the location of the WD2014 ice-core site. Although Laird et al. (2010) suggested that flow-induced disturbance on layer geometry is limited in the area around the WD2014 site, changes in bed roughness were found to affect englacial stratigraphy near WD2014. This could lead to small undulation in IRH elevations between our transect and WD2014 and thus likely result in several meters of discrepancy. To acknowledge this, and considering that the sulphate peaks are most likely the cause of our IRHs as we show above, we have increased the age uncertainty of our IRHs to account for the offset between our IRH ages and the age of the sulphate peaks (see 2.4.1, Table 3). This results in more conservative uncertainties for our deeper three IRHs dated at the ice core: 4.72 ± 0.28 (R2), 6.94 ± 0.31 (R3), and 16.50 ± 0.79 ka (R4).

By linking three of our four IRHs to the sulphate record at WAIS Divide, we can hypothesise that the origin of our spatially-extensive IRHs is from past explosive volcanic activity during the Holocene. Previous studies in Antarctica have demonstrated the correspondence between bright reflectors in radar data and past volcanic activity (e.g. Corr

and Vaughan, 2009; Jacobel and Welch, 2005). Karlsson et al. (2014) previously attempted to link their deeper layer (Layer 2 / R3) to acidity peaks at Byrd ice core, however the absence of a direct link between the PIG catchment and a complete ice-core chronology was lacking at the time. The evidence presented here suggests that our IRHs may also originate from past explosive volcanism, however the precise source of these eruptions, whether regional or global, remains unknown.

4.3 Accumulation Rate and IRH-age Comparison

The correspondence in isochrone-age estimates for IRHs R2-3 derived from intersecting the WD2014 site (Table 3) and using the 1-D model (Table 4) at the PIG/Thwaites divide (~250 km away) (our Sites A and B; Figure 1) suggests that accumulation patterns have remained broadly similar across the Amundsen-Ross divide for at least the last ~7 ka. Whilst this is based on a relatively limited amount of data points, it complements previous studies (Fudge et al., 2016; Koutnik et al., 2016; Neumann et al., 2008), including Siegert and Payne (2004) who, using the same SPRI/NSF/TUD radar transect as that in Figure 1, concluded that accumulation patterns have remained stable over the last 6.4 ka. We suggest future research make use of the accurately dated IRHs provided here to model Holocene accumulation rates and patterns, as well as regional ice-sheet balance velocities, as previously conducted over Greenland (e.g. MacGregor et al., 2016) and on individual sections of the WAIS (Koutnik et al., 2016; Neuman et al., 2008). This will provide additional information on the terrestrial ice-sheet history of the Amundsen Sea Embayment during the Holocene, and in turn help us to constrain better the future of the WAIS.

Previous studies have successfully combined ice-core records with modelled modern-day accumulation rates to reconstruct Holocene accumulation (Cavitte et al., 2018; Fudge et al., 2016; Nielsen et al., 2018), although non-climatic noise in the observations and model biases have resulted in small discrepancies between ice-core and model reconstructions (Cavitte et al., 2020; Dalaiden et al., 2020). When assessing the ability of the 1-D model to reproduce the ages for R2-3 derived at the WD2014 ice-core, we find that the best match (to within < 10%) is achieved using the modern accumulation rates provided by the MED14 and RACMO2 products. This is not surprising as both have higher spatial resolution than MAR and ART06, but it also likely reflects the fact that MED14 is an observational product and that RACMO2 has been shown to agree well with geophysical estimates of accumulation rates (Lenaerts et al., 2012; Medley et al., 2014; van Wessem et al., 2018; Wang et al., 2016). In contrast, when using present-day accumulation estimates from ART06 and MAR to calculate past accumulation rates, model-derived ages are up to 1.1 ka (~23%) greater for R2 and 2.2 ka (~32%) greater for R3 compared with ice-core derived ages (Table 3-4). This discrepancy is primarily dominated by different modern accumulation gradients estimated between WD2014 and the PIG/Thwaites divide (i.e. Site A and B), with the MED14 and RACMO2 products suggesting a slightly more homogenous gradient than ART06 and MAR (Table S4). Lower in the ice, the poor correspondence between the age of R4 derived by links to the WD2014 (16.50 ± 0.79 ka) relative to the age returned by the 1-D model (19.69-26.87 ka) is worthy of investigation. Even taking into account the maximum age uncertainty at the ice core, the minimum and maximum age returned by the 1-D model is 2.6 (15%) and 9.8 ka (57%) greater than at the ice core (Table 3-4), a difference that cannot solely be attributed to the different modern-day accumulation gradients mentioned above. The most likely explanation is that the assumptions required for the 1-D model (see 2.4.2) break down for older IRHs, where local accumulation rate is no longer a primary factor in determining the

depth of an IRH. This could be due to complex flow dynamics such as longitudinal strain or lateral shearing at the boundary between slow and fast-flowing ice, resulting in high internal stress impacting IRH stratigraphy in the deeper part of the ice column (Waddington et al., 2007). Moreover, R4 (16.50 ± 0.79 ka) was deposited pre-Holocene as the WAIS was transitioning from a glacial to an interglacial period during which ice thickness has likely not remained constant (Golledge et al., 2014; Johnson et al., 2017), implying possible changes in ice-flow configurations for which the steady-state model is not able to account.

4.4 Characteristics of Englacial Stratigraphy

Previous research over East Antarctica has shown that common bright reflectors can be interchangeably traced over long distances using radar systems operating at different centre frequencies (Cavitte et al., 2016; Winter et al., 2017). Our findings provide further evidence of this over West Antarctica, having successfully identified common IRHs across different airborne radar systems. However, although IRHs younger than 7 ka can be traced widely across the WAIS using existing data sets, tracing deeper, pre-Holocene IRHs has not been widely possible across PIG (this study) nor the Weddell Sea Sector (Ashmore et al., 2020). Relative to the interior of East Antarctica, where much lower snow accumulation and ice-flow velocities have facilitated the tracing of isochrones pre-dating the Last Glacial Maximum (~ 20 ka BP) and even the past glacial-interglacial periods (up to ~ 366 ka BP) (Cavitte et al., 2016; Parrenin et al., 2017; Steinhage et al., 2013; Winter et al., 2019), the extremely variable deep-ice conditions in the WAIS will challenge the recovery of pre-Holocene radiostratigraphy. Compounding the challenge, Ross et al. (2020) have demonstrated that large packages of ice older than ~ 16 ka in the Weddell Sea sector of the WAIS are rheologically different to the ice above, containing large proportions of deformed and folded ice. These packages typically show poor continuity of englacial stratigraphy across Institute and Möller Ice Streams (Bingham et al., 2015) and, indeed, where we could see IRHs deeper than R4 in PASIN and MCoRDS2 for this study, very few were continuous for long distances. Over other parts of the WAIS, an IRH dating back to 24.9 ± 0.3 ka has been traced in limited radar profiles connecting the Byrd and WAIS divide ice cores, where it was found at 68% and 80% of ice depth at Byrd and WD2014 respectively (Muldoon et al., 2018); however they were also unable to recover deeper continuous IRHs more widely.

Overall, with the existing datasets available across the WAIS, the prospects for tracing and dating Holocene radiostratigraphy widely across the ice sheet with existing data are excellent, but diminish rapidly for older ice, going back to the LGM and beyond. Yet, much deeper, and thus older IRHs, are visible throughout the ice column with ground-based radars (e.g. Bingham et al., 2017; King et al., 2011; Laird et al., 2010) and hence the interrogation of older ice in the WAIS may be best suited to strategic ground campaigns that can be linked into the airborne-derived radiostratigraphy. In the PIG catchment, older ice is suggested by our results to lie below the PIG/Thwaites divide, where on average ~ 900 m of ice (30% of the mean ice thickness) underlies R4 (~ 17 ka) (Figure S5).

5 Conclusion

We have identified four spatially-extensive Internal Reflecting Horizons (IRH) in airborne radar surveys that are present across much of the Pine Island Glacier catchment in West Antarctica. Extending into neighbouring Thwaites Glacier and Institute Ice Stream, these IRHs can be considered isochrones that span the late Pleistocene and Holocene, with ages of 2.31-2.92, 4.72 ± 0.28 , 6.94 ± 0.31 , and 16.50 ± 0.79 ka derived from intersecting the WAIS Divide ice core and the use of a 1-D ice-flow model. Our most spatially-extensive IRH, R2, is remarkably similar in age and depth to another extensive IRH previously identified by other studies over Pine Island Glacier, Institute and Möller Ice Streams, and the Marie Byrd Land region. More broadly, we have also shown that our IRH package is similar to previously-traced IRHs over the Weddell Sea sector of the WAIS, which, together with the Pine Island Glacier catchment represents ~20% of West Antarctica. Lastly, we have shown that our upper three IRHs correspond to large peaks in sulphate concentrations at the WAIS Divide ice core, suggesting that our IRHs are of volcanic origin.

When assessing the presence of older ice across the catchment, we observe that the relative proportion of ice older than R4 in the ice column is limited and does not contain many continuous reflections. Indeed, we find that the deepest (and thus oldest) continuous IRH identified in this study, R4, is found at an average depth of 68% in the ice column despite its age (~17 ka) only representing 25% of the estimated age of the oldest ice recovered at the WAIS Divide ice core (~68 ka). This indicates that the majority of ice older than the LGM is found within the bottom ~30% of the ice thickness across PIG/Upper Thwaites. Whilst this is to be expected as the age-depth profile of an ice sheet does not increase linearly, the absence of continuous reflections dating back to the Last Glacial Maximum and older currently limits our ability to reconstruct longer-term changes using existing airborne data sets.

As isochronous features, the dated IRHs generated here offer a new set of large-scale boundary conditions that could be a valuable resource, if incorporated into ice-flow models seeking to improve our understanding of past ice-sheet evolution. We anticipate that these well-dated IRHs will provide constraints for models simulating past accumulation rates and patterns, which in turn will shed more light onto the terrestrial ice sheet history of this very sensitive catchment of the WAIS.

Acknowledgments

This research was motivated by the AntArchitecture Action Group of the Scientific Committee for Antarctic Research (SCAR). J.A.B. was supported by the NERC Doctoral Training Partnership grant (NE/L002558/1), hosted in the Edinburgh E³ DTP program. We would like to thank the reviewers, Marie Cavitte and T.J. Fudge, for their constructive suggestions which greatly improved this manuscript. We thank the BAS scientists and logistics personnel for acquiring the PASIN data over Pine Island Glacier, which will be made fully available upon publication from the Polar Airborne Geophysics Data Portal of the UK Polar Data Centre (<https://secure.antarctica.ac.uk/data/aerogeo/>). We also thank CReSIS for acquiring and providing the processed MCoRDS2 data, which can be downloaded from the OIB data portal (<https://data.cresis.ku.edu/>). The RACMO2 and MAR SMB outputs were downloaded from (<https://www.projects.science.uu.nl/iceclimate/publications/data/2018>) and (<https://zenodo.org/record/2547638>) respectively. We thank Brooke Medley and Howard Conway for providing the airborne and ground snow accumulation products. Part of the figures included in this paper were produced with outputs from the Antarctic Mapping Toolbox in MATLAB® (Green et al., 2017). The full picking information for each IRH can be downloaded from the UK Polar Data Centre (<https://doi.org/10.5285/f2de31af-9f83-44f8-9584-f0190a2cc3eb>; Bodart et al., 2021).

References

- Arthern, R.J., Winebrenner, D.P. and Vaughan, D.G., 2006. Antarctic snow accumulation mapped using polarization of 4.3-cm wavelength microwave emission. *Journal of Geophysical Research: Atmospheres*, 111(D6). doi: 10.1029/2004JD005667.
- Ashmore, D.W., Bingham, R.G., Ross, N., Siegert, M.J., Jordan, T.A. and Mair, D.W., 2020. Englacial architecture and age-depth constraints across the West Antarctic Ice Sheet. *Geophysical Research Letters*, 47. doi: 10.1029/2019GL086663.
- Bingham, R.G. and Siegert, M.J., 2007. Radio-echo sounding over polar ice masses. *Journal of Environmental and Engineering Geophysics*, 12(1), pp.47-62. doi: 10.2113/JEEG12.1.47
- Bingham, R.G., Rippin, D.M., Karlsson, N.B., Corr, H.F., Ferraccioli, F., Jordan, T.A., Le Brocq, A.M., Rose, K.C., Ross, N. and Siegert, M.J., 2015. Ice-flow structure and ice dynamic changes in the Weddell Sea sector of West Antarctica from radar-imaged internal layering. *Journal of Geophysical Research: Earth Surface*, 120(4), pp.655-670. doi: 10.1002/2014JF003291
- Bingham, R.G., Vaughan, D.G., King, E.C., Davies, D., Cornford, S.L., Smith, A.M., Arthern, R.J., Brisbourne, A.M., Rydt, J., Graham, A.G. and Spagnolo, M., 2017. Diverse landscapes beneath Pine Island Glacier influence ice flow. *Nature communications*, 8(1), p.1618. doi: 10.1038/s41467-017-01597-y
- Bodart, J.A. and Bingham, R.J., 2019. The Impact of the Extreme 2015–2016 El Niño on the Mass Balance of the Antarctic Ice Sheet. *Geophysical Research Letters*, 46(23), pp.13862-13871. doi: 10.1029/2019GL084466
- Bodart, J.A., Bingham, R.G., Ashmore, D.W., Karlsson, N.B., Hein, A.S., and Vaughan, D. G. (2021). *Dated radar stratigraphy of the Pine Island Glacier catchment (West Antarctica) derived from BBAS-PASIN (2004-05) and OIB-MCoRDS2 (2016/2018) surveys*. UK Polar Data Centre, Natural Environment Research Council, UK Research & Innovation. doi: [10.5285/f2de31af-9f83-44f8-9584-f0190a2cc3eb](https://doi.org/10.5285/f2de31af-9f83-44f8-9584-f0190a2cc3eb)
- Bracegirdle, T.J., Colleoni, F., Abram, N.J., Bertler, N.A., Dixon, D.A., England, M., Favier, V., Fogwill, C.J., Fyfe, J.C., Goodwin, I. and Goosse, H., 2019. Back to the future: Using long-term observational and paleo-proxy reconstructions to improve model projections of Antarctic climate. *Geosciences*, 9(6), p.255. doi: 10.3390/geosciences9060255
- Buizert, C., Cuffey, K.M., Severinghaus, J.P., Baggenstos, D., Fudge, T.J., Steig, E.J., Markle, B.R., Winstrup, M., Rhodes, R.H., Brook, E.J. and Sowers, T.A., 2015. The WAIS Divide deep ice core WD2014 chronology—Part 1: Methane synchronization (68–31 kaBP) and the gas age–ice age difference. *Climate of the Past*, 11(2). doi: 10.5194/cp-11-153-2015
- Castellano, E., Becagli, S., Hansson, M., Hutterli, M., Petit, J.R., Rampino, M.R., Severi, M., Steffensen, J.P., Traversi, R. and Udisti, R., 2005. Holocene volcanic history as recorded in the sulfate stratigraphy of the European Project for Ice Coring in Antarctica Dome C (EDC96) ice core. *Journal of Geophysical Research: Atmospheres*, 110(D6). doi: 10.1029/2004JD005259

Catania, G.A., Conway, H., Raymond, C.F. and Scambos, T.A., 2006. Evidence for floatation or near floatation in the mouth of Kamb Ice Stream, West Antarctica, prior to stagnation. *Journal of Geophysical Research: Earth Surface*, 111(F1). doi: 10.1029/2006GL026430

Cavitte, M.G., Blankenship, D.D., Young, D.A., Schroeder, D.M., Parrenin, F., Lemeur, E., Macgregor, J.A. and Siegert, M.J., 2016. Deep radiostratigraphy of the East Antarctic plateau: connecting the Dome C and Vostok ice core sites. *Journal of Glaciology*, 62(232), pp.323-334. doi: 10.1017/jog.2016.11

Cavitte, M.G., Parrenin, F., Ritz, C., Young, D.A., Liefferinge, B., Blankenship, D.D., Frezzotti, M. and Roberts, J., 2018. Accumulation patterns around Dome C, East Antarctica, in the last 73 kyr. *The Cryosphere*, 12, pp.1401-1414. doi: 10.5194/tc-12-1401-2018

Cavitte, M.G., Dalaiden, Q., Goosse, H., Lenaerts, J. and Thomas, E.R., 2020. Reconciling the surface temperature–surface mass balance relationship in models and ice cores in Antarctica over the last two centuries. *The Cryosphere*, 14, 4083–4102, 2020. doi: <https://doi.org/10.5194/tc-14-4083-2020>

Christianson, K., Bushuk, M., Dutrieux, P., Parizek, B.R., Joughin, I.R., Alley, R.B., Shean, D.E., Abrahamsen, E.P., Anandakrishnan, S., Heywood, K.J. and Kim, T.W., 2016. Sensitivity of Pine Island Glacier to observed ocean forcing. *Geophysical Research Letters*, 43(20), pp.10-817. doi: 10.1002/2016GL070500

Clough, J.W., 1977. Radio-echo sounding: reflections from internal layers in ice sheets. *Journal of Glaciology*, 18(78), pp.3-14. doi: 10.3189/S002214300002147X

Cole - Dai, J. (2014) "Major Ion Chemistry Data of WAIS Divide Ice Core Brittle Ice" U.S. Antarctic Program (USAP) Data Center. doi: <https://doi.org/10.7265/N5RF5S0D>.

Corr, H.F. and Vaughan, D.G., 2008. A recent volcanic eruption beneath the West Antarctic ice sheet. *Nature Geoscience*, 1(2), pp.122-125. doi: 10.1038/ngeo106

Conway, H. and Rasmussen, L. A., 2009. Recent thinning and migration of the Western Divide, central West Antarctica. *Geophysical Research Letters*, 36, L12502, doi:10.1029/2009GL038072

CReSIS. 2016. *CReSIS Radar Depth Sounder Data*, Lawrence, Kansas, USA. Digital Media. <http://data.cresis.ku.edu/>

Cuffey, K.M., Clow, G.D., Steig, E.J., Buizert, C., Fudge, T.J., Koutnik, M., Waddington, E.D., Alley, R.B. and Severinghaus, J.P., 2016. Deglacial temperature history of West Antarctica. *Proceedings of the National Academy of Sciences*, 113(50), pp.14249-14254. doi: 10.1073/pnas.1609132113

Dalaiden, Q., Goosse, H., Klein, F., Lenaerts, J., Holloway, M., Sime, L. and Thomas, E.R., 2020. How useful is snow accumulation in reconstructing surface air temperature in Antarctica? A study combining ice core records and climate models. *The Cryosphere*, 14(4). doi: 10.5194/tc-14-1187-2020

- Dansgaard, W. and Johnsen, S.J., 1969. A flow model and a time scale for the ice core from Camp Century, Greenland. *Journal of Glaciology*, 8(53), pp.215-223. doi: 10.3189/S0022143000031208
- DeConto, R.M. and Pollard, D., 2016. Contribution of Antarctica to past and future sea-level rise. *Nature*, 531(7596), pp.591-597. doi: 10.1038/nature17145
- Denton, G.H. and Hughes, T.J., 2002. Reconstructing the Antarctic ice sheet at the Last Glacial Maximum. *Quaternary Science Reviews*, 21(1-3), pp.193-202. doi: 10.1016/S0277-3791(01)00090-7
- Dowdeswell, J.A. and Evans, S., 2004. Investigations of the form and flow of ice sheets and glaciers using radio-echo sounding. *Reports on Progress in Physics*, 67(10), p.1821. doi: 10.1088/0034-4885/67/10/R03
- Dutrieux, P., De Rydt, J., Jenkins, A., Holland, P.R., Ha, H.K., Lee, S.H., Steig, E.J., Ding, Q., Abrahamsen, E.P. and Schröder, M., 2014. Strong sensitivity of Pine Island ice-shelf melting to climatic variability. *Science*, 343(6167), pp.174-178. doi: 10.1126/science.1244341
- Eisen, O., Rack, W., Nixdorf, U. and Wilhelms, F., 2005. Characteristics of accumulation around the EPICA deep-drilling site in Dronning Maud Land, Antarctica. *Annals of Glaciology*, 41, pp.41-46. doi: 10.3189/172756405781813276
- Eisen, O., Frezzotti, M., Genthon, C., Isaksson, E., Magand, O., van den Broeke, M.R., Dixon, D.A., Ekaykin, A., Holmlund, P., Kameda, T. and Karlöf, L., 2008. Ground-based measurements of spatial and temporal variability of snow accumulation in East Antarctica. *Reviews of Geophysics*, 46(2). doi: 10.1029/2006RG000218
- Fahnestock, M., Abdalati, W., Joughin, I., Brozena, J., & Gogineni, P., 2001a. High geothermal heat flow, basal melt, and the origin of rapid ice flow in central Greenland. *Science*, 294(5550), 2238–2342. doi: 10.1126/science.1065370
- Fahnestock, M., Abdalati, W., Luo, S. and Gogineni, S., 2001b. Internal layer tracing and age-depth-accumulation relationships for the northern Greenland ice sheet. *Journal of Geophysical Research: Atmospheres*, 106(D24), pp.33789-33797. doi: 10.1029/2001JD900200
- Favier, L., Durand, G., Cornford, S.L., Gudmundsson, G.H., Gagliardini, O., Gillet-Chaulet, F., Zwinger, T., Payne, A.J. and Le Brocq, A.M., 2014. Retreat of Pine Island Glacier controlled by marine ice-sheet instability. *Nature Climate Change*, 4(2), p.117. doi:10.1038/nclimate2094
- Fudge, T.J., Markle, B.R., Cuffey, K.M., Buizert, C., Taylor, K.C., Steig, E.J., Waddington, E.D., Conway, H. and Koutnik, M., 2016. Variable relationship between accumulation and temperature in West Antarctica for the past 31,000 years. *Geophysical Research Letters*, 43(8), pp.3795-3803. doi: 10.1002/2016GL068356

Fudge, T.J., Biyani, S.C., Clemens-Sewall, D. and Hawley, R.L., 2019. Constraining geothermal flux at coastal domes of the Ross Ice Sheet, Antarctica. *Geophysical Research Letters*, 46(22), pp.13090-13098. doi: 10.1029/2019GL084332

Fujita, S., Maeno, H., Uratsuka, S., Furukawa, T., Mae, S., Fujii, Y. and Watanabe, O., 1999. Nature of radio echo layering in the Antarctic ice sheet detected by a two-frequency experiment. *Journal of Geophysical Research: Solid Earth*, 104(B6), pp.13013-13024. doi: 10.1029/1999JB900034

Fujita, S., Matsuoka, T., Ishida, T., Matsuoka, K., & Mae, S. 2000. A summary of the complex dielectric permittivity of ice in the megahertz range and its applications for radar sounding of polar ice sheets. In T. Hondoh (Ed.), *Physics of ice core records* (pp. 185–212). Sapporo: Hokkaido University Press.

Golledge, N.R., Menviel, L., Carter, L., Fogwill, C.J., England, M.H., Cortese, G. and Levy, R.H., 2014. Antarctic contribution to meltwater pulse 1A from reduced Southern Ocean overturning. *Nature communications*, 5, p.5107. doi: 10.1038/ncomms6107

Gow, A. J. (1970). Preliminary results of studies of ice cores from the 2164m-deep drill hole, Byrd Station, Antarctica, *Antarctic Glaciological Exploration (ISAGE)*, Redbooks (Vol. 86, pp. 78–90). UK: IAHS.

Gow, A.J. and Williamson, T., 1971. Volcanic ash in the Antarctic ice sheet and its possible climatic implications. *Earth and Planetary Science Letters*, 13(1), pp.210-218. doi: 10.1016/0012-821X(71)90126-9

Greene, C. A., Gwyther, D. E., & Blankenship, D. D., 2017. Antarctic Mapping Tools for Matlab. *Computers & Geosciences*. 104, pp.151-157. doi: 10.1016/j.cageo.2016.08.003.

Hammer, C.U., Clausen, H.B. and Langway, C.C., 1997. 50,000 years of recorded global volcanism. *Climatic Change*, 35(1), pp.1-15. doi: 10.1023/A:1005344225434

Harrison, C.H., 1973. Radio echo sounding of horizontal layers in ice. *Journal of glaciology*, 12(66), pp.383-397. doi: 10.3189/S0022143000031804

Hein, A.S., Woodward, J., Marrero, S.M., Dunning, S.A., Steig, E.J., Freeman, S.P., Stuart, F.M., Winter, K., Westoby, M.J. and Sugden, D.E., 2016. Evidence for the stability of the West Antarctic Ice Sheet divide for 1.4 million years. *Nature communications*, 7(1), pp.1-8. doi: 10.1038/ncomms10325

Hillenbrand, C.D., Kuhn, G., Smith, J.A., Gohl, K., Graham, A.G., Larter, R.D., Klages, J.P., Downey, R., Moreton, S.G., Forwick, M. and Vaughan, D.G., 2013. Grounding-line retreat of the west Antarctic ice sheet from inner Pine island Bay. *Geology*, 41(1), pp.35-38. doi: 10.1130/G33469.1

Holschuh, N., Christianson, K. and Anandakrishnan, S., 2014. Power loss in dipping internal reflectors, imaged using ice-penetrating radar. *Annals of glaciology*, 55(67), pp.49-56. doi: 10.3189/2014AoG67A005

- 1025 Holschuh, N., Christianson, K., Conway, H., Jacobel, R.W. and Welch, B.C., 2018.
- 1026 Persistent tracers of historic ice flow in glacial stratigraphy near Kamb Ice Stream, West
- 1027 Antarctica. *The Cryosphere*, 12(9), pp.2821-2829. doi: 10.5194/tc-12-2821-2018
- 1028
- 1029 Holland, P.R., Bracegirdle, T.J., Dutrieux, P., Jenkins, A. and Steig, E.J., 2019. West
- 1030 Antarctic ice loss influenced by internal climate variability and anthropogenic forcing. *Nature*
- 1031 *Geoscience*, 12(9), pp.718-724. doi: 10.1038/s41561-019-0420-9
- 1032
- 1033 Jacobel, R.W., Scambos, T.A., Raymond, C.F. and Gades, A.M., 1996. Changes in
- 1034 the configuration of ice stream flow from the West Antarctic Ice Sheet. *Journal of*
- 1035 *Geophysical Research: Solid Earth*, 101(B3), pp.5499-5504. doi: 10.1029/95JB03735
- 1036
- 1037 Jacobel, R.W. and Welch, B.C., 2005. A time marker at 17.5 ka BP detected
- 1038 throughout West Antarctica. *Annals of Glaciology*, 41, pp.47-51. doi:
- 1039 10.3189/172756405781813348
- 1040
- 1041 Jakobsson, M., Anderson, J.B., Nitsche, F.O., Dowdeswell, J.A., Gyllencreutz, R.,
- 1042 Kirchner, N., Mohammad, R., O'Regan, M., Alley, R.B., Anandakrishnan, S. and Eriksson,
- 1043 B., 2011. Geological record of ice shelf break-up and grounding line retreat, Pine Island Bay,
- 1044 West Antarctica. *Geology*, 39(7), pp.691-694. doi: 10.1130/G32153.1
- 1045
- 1046 Johnson, J.S., Bentley, M.J. and Gohl, K., 2008. First exposure ages from the
- 1047 Amundsen Sea embayment, West Antarctica: The late Quaternary context for recent thinning
- 1048 of Pine Island, Smith, and Pope Glaciers. *Geology*, 36(3), pp.223-226. doi:
- 1049 10.1130/G24207A.1
- 1050
- 1051 Johnson, J.S., Bentley, M.J., Smith, J.A., Finkel, R.C., Rood, D.H., Gohl, K., Balco,
- 1052 G., Larter, R.D. and Schaefer, J.M., 2014. Rapid thinning of Pine Island Glacier in the early
- 1053 Holocene. *Science*, 343(6174), pp.999-1001. doi: 10.1126/science.1247385
- 1054
- 1055 Johnson, J.S., Smith, J.A., Schaefer, J.M., Young, N.E., Goehring, B.M., Hillenbrand,
- 1056 C.D., Lamp, J.L., Finkel, R.C. and Gohl, K., 2017. The last glaciation of Bear Peninsula,
- 1057 central Amundsen Sea Embayment of Antarctica: Constraints on timing and duration
- 1058 revealed by in situ cosmogenic ¹⁴C and ¹⁰Be dating. *Quaternary Science Reviews*, 178,
- 1059 pp.77-88. doi: 10.1016/j.quascirev.2017.11.003
- 1060
- 1061 Johnson, J.S., Roberts, S.J., Rood, D.H., Pollard, D., Schaefer, J.M., Whitehouse,
- 1062 P.L., Ireland, L.C., Lamp, J.L., Goehring, B.M., Rand, C. and Smith, J.A., 2020. Deglaciation
- 1063 of Pope Glacier implies widespread early Holocene ice sheet thinning in the Amundsen Sea
- 1064 sector of Antarctica. *Earth and Planetary Science Letters*, 548, p.116501. doi:
- 1065 10.1016/j.epsl.2020.116501
- 1066
- 1067 Karlsson, N.B., Rippin, D.M., Vaughan, D.G. and Corr, H.F., 2009. The internal
- 1068 layering of Pine Island Glacier, West Antarctica, from airborne radar-sounding data. *Annals*
- 1069 *of Glaciology*, 50(51), pp.141-146. doi:10.3189/S0260305500250660
- 1070
- 1071 Karlsson, N.B., Rippin, D.M., Bingham, R.G. and Vaughan, D.G., 2012. A
- 1072 'continuity-index' for assessing ice-sheet dynamics from radar-sounded internal layers. *Earth*
- 1073 *and Planetary Science Letters*, 335, pp.88-94. doi: 10.1016/j.epsl.2012.04.034
- 1074

- 1075 Karlsson, N.B., Bingham, R.G., Rippin, D.M., Hindmarsh, R.C., Corr, H.F. and
1076 Vaughan, D.G., 2014. Constraining past accumulation in the central Pine Island Glacier
1077 basin, West Antarctica, using radio-echo sounding. *Journal of Glaciology*, 60(221), pp.553-
1078 562. doi: 10.3189/2014JoG13j180
- 1079
1080 King, E., 2011. Ice stream or not? Radio-echo sounding of Carlson Inlet, West
1081 Antarctica. *The Cryosphere*, 5(4), pp.907-916. doi: 10.5194/tc-5-907-2011
- 1082
1083 King, E.C., 2020. The precision of radar-derived subglacial bed topography: a case
1084 study from Pine Island Glacier, Antarctica. *Annals of Glaciology*, pp.1-8. doi:
1085 10.1017/aog.2020.33
- 1086
1087 Kingslake, J., Scherer, R.P., Albrecht, T., Coenen, J., Powell, R.D., Reese, R.,
1088 Stansell, N.D., Tulaczyk, S., Wearing, M.G. and Whitehouse, P.L., 2018. Extensive retreat
1089 and re-advance of the West Antarctic Ice Sheet during the Holocene. *Nature*, 558(7710),
1090 p.430. doi: 10.1038/s41586-018-0208-x
- 1091
1092 Konrad, H., Gilbert, L., Cornford, S.L., Payne, A., Hogg, A., Muir, A. and Shepherd,
1093 A., 2017. Uneven onset and pace of ice-dynamical imbalance in the Amundsen Sea
1094 Embayment, West Antarctica. *Geophysical Research Letters*, 44(2), pp.910-918. Doi:
1095 10.1002/2016GL070733
- 1096
1097 Koutnik, M.R., Fudge, T.J., Conway, H., Waddington, E.D., Neumann, T.A., Cuffey,
1098 K.M., Buizert, C. and Taylor, K.C., 2016. Holocene accumulation and ice flow near the West
1099 Antarctic Ice Sheet Divide ice core site. *Journal of Geophysical Research: Earth Surface*,
1100 121(5), pp.907-924. doi: 10.1002/2015JF003668
- 1101
1102 Laird, C.M., Blake, W.A., Matsuoka, K., Conway, H., Allen, C.T., Leuschen, C.J. and
1103 Gogineni, S., 2010. Deep ice stratigraphy and basal conditions in central West Antarctica
1104 revealed by coherent radar. *IEEE Geoscience and Remote Sensing Letters*, 7(2), pp.246-250.
1105 doi: 10.1109/LGRS.2009.2032304
- 1106
1107 Lenaerts, J.T., Van den Broeke, M.R., Van de Berg, W.J., Van Meijgaard, E. and
1108 Kuipers Munneke, P., 2012. A new, high-resolution surface mass balance map of Antarctica
1109 (1979–2010) based on regional atmospheric climate modeling. *Geophysical Research Letters*,
1110 39(4). doi: 10.1029/2011GL050713
- 1111
1112 Leysinger Vieli, G.J.M., Hindmarsh, R.C., Siegert, M.J. and Bo, S., 2011. Time-
1113 dependence of the spatial pattern of accumulation rate in East Antarctica deduced from
1114 isochronic radar layers using a 3-D numerical ice flow model. *Journal of Geophysical
1115 Research: Earth Surface*, 116(F2). doi: 10.1029/2010JF001785
- 1116
1117 Lindow, J., Castex, M., Wittmann, H., Johnson, J.S., Lisker, F., Gohl, K. and Spiegel,
1118 C., 2014. Glacial retreat in the Amundsen Sea sector, West Antarctica—first cosmogenic
1119 evidence from central Pine Island Bay and the Kohler Range. *Quaternary Science Reviews*,
1120 98, pp.166-173. doi: 10.1016/j.quascirev.2014.05.010
- 1121
1122 Lliboutry, L. A. (1979). A critical review of analytical approximate solutions for
1123 steady state velocities and temperatures in cold ice sheets. *Gletscherkd. Glazialgeol*, 15, 135–
1124 148

- Lowe, A.L. and Anderson, J.B., 2002. Reconstruction of the West Antarctic ice sheet in Pine Island Bay during the Last Glacial Maximum and its subsequent retreat history. *Quaternary Science Reviews*, 21(16-17), pp.1879-1897. doi: 10.1016/S0277-3791(02)00006-9
- MacGregor, J.A., Fahnestock, M.A., Catania, G.A., Paden, J.D., Gogineni, S.P., Young, S.K., Rybarski, S.C., Mabrey, A.N., Wagman, B.M. and Morlighem, M., 2015. Radiostratigraphy and age structure of the Greenland Ice Sheet. *Journal of Geophysical Research: Earth Surface*, 120(2), pp.212-241. doi: 10.1002/2014JF003215
- MacGregor, J.A., Colgan, W.T., Fahnestock, M.A., Morlighem, M., Catania, G.A., Paden, J.D. and Gogineni, S.P., 2016. Holocene deceleration of the Greenland ice sheet. *Science*, 351(6273), pp.590-593. doi: 10.1126/science.aab1702
- McConnell, J.R., Burke, A., Dunbar, N.W., Köhler, P., Thomas, J.L., Arienzo, M.M., Chellman, N.J., Maselli, O.J., Sigl, M., Adkins, J.F. and Baggenstos, D., 2017. Synchronous volcanic eruptions and abrupt climate change~ 17.7 ka plausibly linked by stratospheric ozone depletion. *Proceedings of the National Academy of Sciences*, 114(38), pp.10035-10040. doi: 10.1073/pnas.1705595114
- Medley, B., Joughin, I.R., Smith, B.E., Das, S.B., Steig, E.J., Conway, H., Gogineni, S., Lewis, C.S., Criscitiello, A.S., McConnell, J.R. and van den Broeke, M.R., 2014. Constraining the recent mass balance of Pine Island and Thwaites glaciers, West Antarctica, with airborne observations of snow accumulation. *The Cryosphere*, 8, 1375–1392. doi: 10.5194/tc-8-1375-2014
- Medley, B., McConnell, J.R., Neumann, T.A., Reijmer, C.H., Chellman, N., Sigl, M. and Kipfstuhl, S., 2018. Temperature and snowfall in western Queen Maud Land increasing faster than climate model projections. *Geophysical Research Letters*, 45(3), pp.1472-1480. doi: 10.1002/2017GL075992
- Millar, D.H.M., 1981. Radio-echo layering in polar ice sheets and past volcanic activity. *Nature*, 292(5822), pp.441-443. doi: 10.1038/292441a0
- Millar, D.H.M., 1982. Acidity levels in ice sheets from radio echo-sounding. *Annals of Glaciology*, 3, pp.199-203. doi: 10.3189/S0260305500002779
- Moore, J.C., 1988. Dielectric variability of a 130 m Antarctic ice core: implications for radar sounding. *Annals of Glaciology*, 11, pp.95-99. doi: 10.3189/S026030550000639X
- Morlighem, M., Rignot, E., Binder, T., Blankenship, D., Drews, R., Eagles, G., Eisen, O., Ferraccioli, F., Forsberg, R., Fretwell, P. and Goel, V., 2020. Deep glacial troughs and stabilizing ridges unveiled beneath the margins of the Antarctic ice sheet. *Nature Geoscience*, 13(2), pp.132-137. doi: 10.1038/s41561-019-0510-8
- Muldoon, G.R., 2018. *West Antarctic Ice Sheet retreat during the Last Interglacial* (Doctoral dissertation). Retrieved from The University of Texas at Austin ScholarWorks Repository. (<http://hdl.handle.net/2152/65631>). Location: University of Texas at Austin.

- Muldoon, G.R., Jackson, C.S., Young, D.A. and Blankenship, D.D., 2018. Bayesian estimation of englacial radar chronology in Central West Antarctica. *Dynamics and Statistics of the Climate System*, 3(1), p.dzy004. doi: 10.1093/climatesystem/dzy004
- Nielsen, L.T., Aðalgeirsdóttir, G., Gkinis, V., Nuterman, R. and Hvidberg, C.S., 2018. The effect of a Holocene climatic optimum on the evolution of the Greenland ice sheet during the last 10 kyr. *Journal of Glaciology*, 64(245), pp.477-488. doi: 10.1017/jog.2018.40
- Neumann, T.A., Conway, H., Price, S.F., Waddington, E.D., Catania, G.A. and Morse, D.L., 2008. Holocene accumulation and ice sheet dynamics in central West Antarctica. *Journal of Geophysical Research: Earth Surface*, 113(F2). doi: 10.1029/2007JF000764
- Nye, J.F., 1957. The distribution of stress and velocity in glaciers and ice-sheets. *Proceedings of the Royal Society of London. Series A. Mathematical and Physical Sciences*, 239(1216), pp.113-133. doi: 10.1098/rspa.1957.0026
- Palermé, C., Genthon, C., Claud, C., Kay, J.E., Wood, N.B. and L'Ecuyer, T., 2017. Evaluation of current and projected Antarctic precipitation in CMIP5 models. *Climate dynamics*, 48(1-2), pp.225-239. doi: 10.1007/s00382-016-3071-1
- Parrenin, F., Cavitte, M.G., Blankenship, D.D., Chappellaz, J., Fischer, H., Gagliardini, O., Masson-Delmotte, V., Passalacqua, O., Ritz, C., Roberts, J. and Siegert, M.J., 2017. Is there 1.5-million-year-old ice near Dome C, Antarctica?. *The Cryosphere*, 11(6), pp.2427-2437. doi: 10.5194/tc-11-2427-2017
- Rignot, E., J. Mouginot, and B. Scheuchl. 2017. *MEaSURES InSAR-Based Antarctica Ice Velocity Map, Version 2*. Boulder, Colorado USA. NASA National Snow and Ice Data Center Distributed Active Archive Center. doi: 10.5067/D7GK8F5J8M8R.
- Rignot, E., Mouginot, J., Scheuchl, B., van den Broeke, M., van Wessem, M.J. and Morlighem, M., 2019. Four decades of Antarctic Ice Sheet mass balance from 1979–2017. *Proceedings of the National Academy of Sciences*, 116(4), pp.1095-1103. doi: 10.1073/pnas.1812883116
- Ritz, C., Rommelaere, V. and Dumas, C., 2001. Modeling the evolution of Antarctic ice sheet over the last 420,000 years: Implications for altitude changes in the Vostok region. *Journal of Geophysical Research: Atmospheres*, 106(D23), pp.31943-31964. doi: 10.1029/2001JD900232
- Ross, N., Siegert, M.J., Woodward, J., Smith, A.M., Corr, H.F., Bentley, M.J., Hindmarsh, R.C., King, E.C. and Rivera, A., 2011. Holocene stability of the Amundsen-Weddell ice divide, West Antarctica. *Geology*, 39(10), pp.935-938. doi :10.1130/G31920
- Ross, N., Bingham, R. G., Corr, H. F. J., Ferraccioli, F., Jordan, T. A., Le Brocq, A., et al. (2012). Steep reverse bed slope at the grounding line of the Weddell Sea sector in West Antarctica. *Nature Geoscience*, 5, 393–396. doi: 10.1038/ngeo1468

- 1223 Ross, N., Corr, H. and Siegert, M., 2020. Large-scale englacial folding and deep-ice
1224 stratigraphy within the West Antarctic Ice Sheet. *The Cryosphere*, 14, pp. 2103–2114. doi:
1225 10.5194/tc-14-2103-2020
- 1226
- 1227 Rotschky, G., Eisen, O., Wilhelms, F., Nixdorf, U. and Oerter, H., 2004. Spatial
1228 distribution of surface mass balance on Amundsenisen plateau, Antarctica, derived from ice-
1229 penetrating radar studies. *Annals of Glaciology*, 39, pp.265-270. doi:
1230 10.3189/172756404781814618
- 1231
- 1232 Scambos, T.A., Haran, T.M., Fahnestock, M.A., Painter, T.H. and Bohlander, J.,
1233 2007. MODIS-based Mosaic of Antarctica (MOA) data sets: Continent-wide surface
1234 morphology and snow grain size. *Remote sensing of environment*, 111(2-3), pp.242-257. doi:
1235 10.1016/j.rse.2006.12.020
- 1236
- 1237 Schroeder, D.M., Dowdeswell, J.A., Siegert, M.J., Bingham, R.G., Chu, W., MacKie,
1238 E.J., Siegfried, M.R., Vega, K.I., Emmons, J.R. and Winstein, K., 2019. Multidecadal
1239 observations of the Antarctic ice sheet from restored analog radar records. *Proceedings of the*
1240 *National Academy of Sciences*, 116(38), pp.18867-18873. doi: 10.1073/pnas.1821646116
- 1241
- 1242 Schwander, J., Jouzel, J., Hammer, C.U., Petit, J.R., Udisti, R. and Wolff, E., 2001. A
1243 tentative chronology for the EPICA Dome Concordia ice core. *Geophysical Research Letters*,
1244 28(22), pp.4243-4246. doi: 10.1029/2000GL011981
- 1245
- 1246 Shepherd, A., Ivins, E. R., Rignot, E., Smith, B., Van Den Broeke, M., Velicogna, I.,
1247 et al. (2018). Mass balance of the Antarctic Ice Sheet from 1992 to 2017. *Nature*, 556, 219–
1248 222. doi: 10.1038/s41586-018-0179-y
- 1249
- 1250 Siegert, M.J., Hodgkins, R. and Dowdeswell, J.A., 1998. A chronology for the Dome
1251 C deep ice-core site through radio-echo layer Correlation with the Vostok Ice Core,
1252 Antarctica. *Geophysical Research Letters*, 25(7), pp.1019-1022. doi: 10.1029/98GL00718
- 1253
- 1254 Siegert, M.J. and Payne, A.J., 2004. Past rates of accumulation in central West
1255 Antarctica. *Geophysical Research Letters*, 31(12). doi: 10.1029/2004GL020290
- 1256
- 1257 Siegert, M.J., Pokar, M., Dowdeswell, J.A. and Benham, T., 2005. Radio-echo
1258 layering in West Antarctica: a spreadsheet dataset. *Earth Surface Processes and Landforms:*
1259 *The Journal of the British Geomorphological Research Group*, 30(12), pp.1583-1591. doi:
1260 10.1002/esp.1238
- 1261
- 1262 Siegert, M., Ross, N., Corr, H., Kingslake, J. and Hindmarsh, R., 2013. Late Holocene
1263 ice-flow reconfiguration in the Weddell Sea sector of West Antarctica. *Quaternary Science*
1264 *Reviews*, 78, pp.98-107. doi: 10.1016/j.quascirev.2013.08.003
- 1265
- 1266 Sigl, M., Fudge, T.J., Winstrup, M., Cole-Dai, J., Ferris, D., McConnell, J.R., Taylor,
1267 K.C., Welten, K.C., Woodruff, T.E., Adolphi, F. and Bisiaux, M., 2016. The WAIS Divide
1268 deep ice core WD2014 chronology–Part 2: Annual-layer counting (0–31 ka BP). *Climate of*
1269 *the Past*, 12(3), pp.769-786. doi: 10.5194/cp-12-769-2016
- 1270
- 1271 Smith, J.A., Andersen, T.J., Shortt, M., Gaffney, A.M., Truffer, M., Stanton, T.P.,
1272 Bindshadler, R., Dutrieux, P., Jenkins, A., Hillenbrand, C.D. and Ehrmann, W., 2017. Sub-

ice-shelf sediments record history of twentieth-century retreat of Pine Island Glacier. *Nature*, 541(7635), pp.77-80. doi: 10.1038/nature20136

Steinhage, D., Kipfstuhl, S., Nixdorf, U. and Miller, H., 2013. Internal structure of the ice sheet between Kohnen station and Dome Fuji, Antarctica, revealed by airborne radio-echo sounding. *Annals of Glaciology*, 54(64), pp.163-167. doi: 10.3189/2013AoG64A113

van Wessem, J.M., Jan Van De Berg, W., Noël, B.P., Van Meijgaard, E., Amory, C., Birnbaum, G., Jakobs, C.L., Krüger, K., Lenaerts, J., Lhermitte, S. and Ligtenberg, S.R., 2018. Modelling the climate and surface mass balance of polar ice sheets using RACMO2: Part 2: Antarctica (1979-2016). *The Cryosphere*, 12(4), pp.1479-1498. doi.org/10.5194/tc-12-1479-2018

Vaughan, D.G., Corr, H.F., Ferraccioli, F., Frearson, N., O'Hare, A., Mach, D., Holt, J.W., Blankenship, D.D., Morse, D.L. and Young, D.A., 2006. New boundary conditions for the West Antarctic ice sheet: Subglacial topography beneath Pine Island Glacier. *Geophysical Research Letters*, 33(9). doi: 10.1029/2005GL025588

Waddington, E.D., Conway, H., Steig, E.J., Alley, R.B., Brook, E.J., Taylor, K.C. and White, J.W.C., 2005. Decoding the dipstick: thickness of Siple Dome, West Antarctica, at the last glacial maximum. *Geology*, 33(4), pp.281-284. doi: 10.1130/G21165.1

Waddington, E.D., Neumann, T.A., Koutnik, M.R., Marshall, H.P. and Morse, D.L., 2007. Inference of accumulation-rate patterns from deep layers in glaciers and ice sheets. *Journal of Glaciology*, 53(183), pp.694-712. doi: 10.3189/002214307784409351

Wang, Y., Ding, M., Van Wessem, J.M., Schlosser, E., Altnau, S., van den Broeke, M.R., Lenaerts, J.T., Thomas, E.R., Isaksson, E., Wang, J. and Sun, W., 2016. A comparison of Antarctic Ice Sheet surface mass balance from atmospheric climate models and in situ observations. *Journal of Climate*, 29(14), pp.5317-5337. doi: 10.1175/JCLI-D-15-0642.1

Whillans, I.M., 1976. Radio-echo layers and the recent stability of the West Antarctic ice sheet. *Nature*, 264(5582), pp.152-155. doi: 10.1038/264152a0

Winter, A., Steinhage, D., Arnold, E.J., Blankenship, D.D., Cavitte, M.G., Corr, H.F., Paden, J.D., Urbini, S., Young, D.A. and Eisen, O., 2017. Comparison of measurements from different radio-echo sounding systems and synchronization with the ice core at Dome C, Antarctica. *The Cryosphere*, 11(1), pp.653-668. doi: 10.5194/tc-11-653-2017

Winter, A., Steinhage, D., Creyts, T.T., Kleiner, T. and Eisen, O., 2019. Age stratigraphy in the East Antarctic Ice Sheet inferred from radio-echo sounding horizons. *Earth System Science Data*, 11(3), pp.1069-1081. doi: 10.5194/essd-11-1069-2019

Zwally, H. J., Giovinetto, M. B., Beckley, M. A., & Saba, J. L. (2012). *Antarctic and Greenland drainage systems*, GSFC Cryospheric Sciences Laboratory. Retrieved from https://icesat4.gsfc.nasa.gov/cryo_data/ant_grn_drainage_systems.php